

Statistical characterization of free-stream turbulence induced transition

Statistical characterization of free-stream turbulence induced transition under variable Reynolds number, free-stream turbulence and pressure gradient

M. Dellacasagrande,^{1, a)} D. Lengani,¹ D. Simoni,¹ J. O. Pralits,² K. Durovich,³ A. Hanifi,³ and D. Henningson³

¹⁾DIME - Università di Genova, Via Montallegro 1, 16145 Genoa, Italy

²⁾DICCA - Università di Genova, Via Montallegro 1, 16145 Genoa, Italy

³⁾Linné Flow Centre, KTH Mechanics, SE-100 44 Stockholm, Sweden

(Dated: 31 August 2021)

In this work, the free-stream turbulence (FST) induced transition of a flat plate boundary layer is studied using particle image velocimetry (PIV) under variable Reynolds number (Re), FST intensity and adverse pressure gradient (APG). Overall, 10 different flow conditions were tested concerning the variation of these parameters. The streak spacing and the probability density function (PDF) of turbulent spot nucleation are computed for all cases. The streak spacing is shown to be constant in the transition region once scaled with the turbulent displacement and momentum thickness, with resulting values of around 3 and 5, respectively. Nucleation events are shown to occur near the position where the dimensionless streak spacing reaches such constant values. The streamwise position where most of turbulent spots are formed is strongly influenced by the FST intensity level. Additionally, the PDF of spot nucleation becomes narrower increasing the APG, while FST has the opposite effect. A common distribution of all the PDFs is provided as a function of a similarity variable accounting for the streak spacing, the shape factor of the boundary layer and the FST intensity.

Keywords: FST induced transition - Turbulent spots nucleation - Multi-plane PIV measurements

I. INTRODUCTION

The transition of a boundary layer subject to free-stream turbulence is driven by the growth and the successive breakup of unsteady streaky structures (see Westin et al.¹, Kendall²). Streaks develop as longitudinal low-frequency perturbations in the laminar boundary layer, with a well defined spanwise scale (see, e.g., Matsubara and Alfredsson³). Once formed, streaks are amplified and then break down leading to the generation of turbulent spots (see Emmons⁴), which convect and merge, causing the transition completion. Due to the inherent sensitivity of the transition process to the external flow characteristics (FST intensity and integral length scale, Reynolds number and pressure gradient), the path to turbulence in a boundary layer subject to FST is an extremely complex phenomenon (see among others Matsubara and Alfredsson³, Brandt et al.⁵, Fransson et al.⁶, Nolan and Zaki⁷, Fransson and Shahinfar⁸), which is still to be fully understood.

In the case of FST induced transition, velocity disturbances penetrate the laminar boundary layer from the free-stream region according to the *shear sheltering* mechanism described in Hunt and Durbin⁹, Jacob and Durbin¹⁰ and Zaki and Saha¹¹. High frequency fluctuations are filtered by the boundary layer, while low frequency high amplitude disturbances penetrate the near wall region (see Wang et al.¹²). Sundaram et al.¹³ studied the response of a semi-infinite flat plate BL to deterministic free-stream excitation, which is different from other studies concerning the role of FST on transition. The

flow was shown to be more receptive with higher strength of disturbance. In the laminar region, the scales of disturbances are sensibly larger than the boundary layer dimension. As streaks propagate in the main flow direction, their spanwise scale becomes comparable with the boundary layer thickness (see Matsubara and Alfredsson³) and their energy increases. Kendall² and Westin et al.¹ showed that the energy of streamwise fluctuations in the boundary layer grows linearly with x (being x the main direction of the flow) until breakup occurs (see also Brandt et al.⁵).

When streaks reach a certain amplitude, secondary instability can occur. Unstable streaks exhibit time dependent fluctuations (Swearingen and Blackwelder¹⁴) which can occur in both symmetric (varicose) and antisymmetric (sinuous) configurations (see e.g., Andersson et al.¹⁵, Brandt and Henningson¹⁶, Asai et al.¹⁷, Mans et al.¹⁸ and Schlatter et al.¹⁹), with this latter being the most dangerous one in terms of promoting transition (Andersson et al.¹⁵, Mans et al.²⁰). Andersson et al.¹⁵ found that the critical streak amplitude leading to the occurrence of sinuous unstable modes is 26% of free-stream velocity, whereas a value of 37% was observed for the varicose mode (similar results were found in the more recent work of Zhang et al.²¹). Brandt et al.⁵ performed direct numerical simulations showing that streak instability is driven by the strong shear associated with the presence of adjacent high- and low-speed filaments. Inviscid instability is found to dominate the breakup process, with high frequency modes forming close to the boundary layer edge. In the more recent work of Brandt and De Lange²², the role of streak interaction in the formation of the turbulent spot was inspected using direct numerical simulations under zero pressure gradient. The authors demonstrated that the collision of two boundary

^{a)}Electronic mail: matteo.dellacasagrande@edu.unige.it

layer streaks can cause their breakup without the addition of background noise. Mans et al.¹⁸ analyzed the sinuous instability of streaks forming in a flat plate boundary layer at constant Reynolds number and FST intensity. They found that the streamwise and spanwise wavelengths of sinuous mode instability scale with the boundary layer thickness (see also Mans et al.²⁰). In the more recent paper of Zhang et al.²¹ the role of high-frequency free-stream turbulence disturbances in promoting streak secondary instability was discussed in details. The authors showed that even with weak intensity, streaks are susceptible to the high-frequency free-stream vortical disturbances. The authors show that streak secondary instability is excited by the nonlinear interaction between the high-frequency free-stream disturbances and the non-parallel streak base flow. Regardless of the dominant mechanism driving the breakup process of streaky structures, the secondary instability of BL streaks leads to the successive formation of turbulent spots (see e.g., Emmons⁴, Brandt and Henningson¹⁶, Mans et al.²⁰ Nolan and Zaki⁷, Marxen and Zaki²³). These latter are known to spread and merge causing transition completion. Goldstein et al.²⁴ examined the spreading of turbulent spots into a Blasius boundary layer showing that the spreading mechanism occurs at the edge of the turbulent region in discrete steps in which new streamwise vortices are formed. The growth characteristics and the shape of spots in boundary layer flows depend on the Reynolds number, pressure gradient, surface roughness and free-stream turbulence level (see the comprehensive work of Lee and Jiang²⁵). Klotz and Wesfreid²⁶ performed the experimental study of spatial and temporal evolution of the transient amplification and subsequent decay of localized spots in plane Couette–Poiseuille flow. The authors demonstrated that the temporal evolution of a localized spot triggered by a well-controlled external perturbation can be explained by linear theory. However, when the Reynolds number and/or amplitude are high enough, the validity of the linear theory is lost.

All the aforementioned works provide a detailed description of the different stages of transition from the receptivity process leading to streaks formation, to their subsequent amplification and their breakup into turbulent spots. However, the characterization of the entire transition process, at least from the statistical point of view, and the description of the combined effects due to the variation of the main influencing parameters (i.e. Reynolds number, FST and pressure gradient) is typically provided by comparing different investigations found in the literature.

The effects due to Reynolds number variation on FST induced transition has not been extensively studied due to the limited spatial resolution of experiments at elevated Reynolds numbers and, further, to the high cost of DNS analysis. Among others, Herson et al.²⁷ performed hot-wire measurements of transitional boundary layer evolving over a flat plate for different values of both the Reynolds number and the FST intensity. The authors found that the penetration depth of disturbances in the boundary layer is inversely proportional to the local Reynolds number, according to the theoretical results obtained by Jacobs and Durbin²⁸ based on solutions of the Orr–Sommerfeld equation. Nolan and Walsh²⁹ showed

that the transition onset position move upstream increasing the Reynolds number, and the boundary layer becomes more receptive to free-stream turbulence (see also the previous work of Jacobs and Durbin²⁸).

The role of free-stream turbulence characteristics in FST induced transition was studied in detail in the past works of Matsumura and Alfredsson³, Brandt et al.⁵, Fransson et al.⁶ and in the more recent work of Fransson and Shahinfar⁸. Brandt et al.⁵ showed that for a Blasius boundary layer, the spanwise scale of streaky structures is only slightly affected by the FST intensity while the increase of its integral length scale delay transition. Fransson et al.⁶ found that the transitional Reynolds number is inversely proportional to the energy of FST, even if for turbulence intensity higher than 2.5% the transition length increases with the energy of fluctuations. Ruan et al.³⁰ performed large eddy simulation of flat plate boundary layer with impinging wakes at different reduced frequency. At higher reduced frequency, i.e. increasing the statistical persistence of wake related turbulence, the length of transition was found to increase. In the recent work of Fransson and Shahinfar⁸, the authors performed hot-wire measurements for a vast range of FST conditions under zero pressure gradient. The authors showed that depending on the intensity of fluctuations, increasing the integral length scale can lead to higher or even lower transitional Reynolds number (see also the recent work of Albiez et al.³¹ in case of adverse pressure gradient). Veerasamy et al.³² studied the effects of non-impinging turbulent wake on the laminar-turbulent transition of a flat plate boundary layer. Reducing the FST experienced by the laminar boundary layer shifts the origin of the streaky structure downstream, thus delaying transition. Additionally, the spanwise scale of the streaky structures is found to correlate with the forcing turbulence characteristics penetrating through the boundary layer edge.

Zaki and Durbin³³ investigated the role of pressure gradient on continuous mode transition using linear theory and numerical simulations. They found that the adverse pressure gradient promotes the receptivity of the boundary layer to low frequency disturbances, thus enhancing the formation of boundary layer streaks. The authors found that early transition occurs in case of an adverse pressure gradient. Nolan and Zaki⁷ computed the probability density function of turbulent spot nucleation for positive, zero and adverse pressure gradient at constant Reynolds number and FST intensity. The authors showed that transition is shortened under strong adverse pressure gradient with nucleation events being localized in a narrow spatial window. Additionally, Zaki³⁴ showed that turbulent spots in adverse pressure gradient flows convect at a lower speed than in accelerated flows, and the spread angle increases. In the more recent work of Wang et al.³⁵ near-wall streaks were found to be more elongated in the streamwise direction with wider spanwise spacing in case of favorable pressure gradient, which leads to an attenuated meandering effect compared to the zero pressure gradient condition. Suryanarayanan et al.³⁶ performed direct numerical simulations of roughness-induced transition in pressure gradient boundary layers. The lift-up and the subsequent amplification of the unsteady perturbations in the BL were found to be mitigated

by flow acceleration. These works provide an overview of the effects of the streamwise pressure gradient on transitional boundary layers, but the combined effects of FST and the flow Reynolds number on the laminar-turbulent transition are not discussed.

In order to obtain the statistical description of the transition process, physical structures evolving from the laminar to the turbulent region have to be recognized and somehow tracked (see the comprehensive review of flow structures in transitional and turbulent flows by Lee and Jiang²⁵). In this sense, discrimination between turbulent and laminar structures is an important task, thus several different approaches have been tested in previous literature works. Among others, Veerasamy and Atkin³⁷ discussed the problem of subjective selection of the threshold value for discrimination between laminar and turbulent flow, proposing an objective approach based on the assumption that the magnitude of the laminar perturbations remains constant throughout the transition region. Differently, Nolan and Zaki⁷ used an Otsu based method (Otsu³⁸) for discriminating between laminar and turbulent events, which is also adopted in the present work for the identification of turbulent spots nucleation (see also the works of Fransson et al.⁶, Kreilos et al.³⁹, Lee and Zaki⁴⁰, Sengupta et al.⁴¹ for an overview of turbulence detection methods).

The present paper aims at the statistical characterization of the FST induced transition under variable Reynolds number, FST intensity level and pressure gradient, showing the effects due to the combined variation of these three parameters. The similarity properties of the spanwise scale of boundary layer streaks in the laminar and the transition region and the streamwise distribution of turbulent spot nucleations are investigated using experimental data obtained from time-resolved PIV measurements. To this end, a turbulent events recognition technique is implemented, which is shown to capture the formation of turbulent spots. The statistical characterization of the main boundary layer structures and of their breakup process leading to the transition completion is therefore provided. The paper is organized as follows: in section II, the experimental setup and the data analysis procedures are presented, discussing the method used for the detection of turbulent events and turbulent spot nucleation. In sections III and IV, the time-averaged and instantaneous PIV results are presented for the different conditions tested to show the time averaged and the instantaneous response of the boundary layer to Re , FST intensity and the adverse pressure gradient variation. In section V, we present the response of the spanwise and streamwise length scales of streaky structures to the flow parameters variation as well as their similarity properties. In section VI, PDFs of turbulent spot nucleations are presented and a similarity variable is introduced to provide a common distribution for all cases. Finally, section VII presents the concluding remarks.

TABLE I: Pressure gradient parameter $k = \frac{v}{U_\infty^2} \frac{dU_\infty}{dx}$ measured at $x/L = 0.3$ for all cases.

| Re | $\alpha = 5deg$ | $\alpha = 9deg$ | $\alpha = 12deg$ |
|------|-----------------|-----------------|------------------|
| 70k | -5.6E-06 | -6.3E-06 | - |
| 150k | -1.3E-06 | -2.2E-06 | -3.9E-06 |
| 220k | -7.1E-07 | -1.3E-06 | -1.7E-06 |

II. EXPERIMENTAL APPARATUS

A. Test section and data matrix

The present experiments were carried out in the open loop low-speed wind tunnel of the Aerodynamics and Turbomachinery Laboratory of the University of Genova. The test section consists of a flat plate with elliptic (4:1) leading edge and a sharp trailing edge. The plate is 300 mm long and 300 mm wide, and it is installed between two symmetric adjustable endwalls (figure 1) allowing the modification of the streamwise pressure gradient. The top surface of the plate has 51 pressure taps. The test section is equipped with optical accesses that allow performing PIV measurements in planes oriented both normal and parallel to the plate surface.

The opening angle of the top surface was set to $\alpha = 5, 9$ and 12 degrees for the present experiments, varying the adverse pressure gradient imposed to the boundary layer. Table I reports the values of the pressure gradient parameter $k = \frac{v}{U_\infty^2} \frac{dU_\infty}{dx}$ measured at $x/L = 0.3$ for all cases. Due to the elevated opening angles of the channel, a trip wire was used to trigger the boundary layer transition on the endwalls in order to avoid boundary layer separation on these surfaces. The free-stream turbulence intensity (Tu) was varied using 3 turbulence generating grids with different geometries. The grids were located 500 mm upstream of the plate leading edge. The turbulence level measured at the channel throat varied in the range 2.5-5% (details of the grids adopted are provided in table II). For the highest FST intensity level and all the pressure gradients, 3 Reynolds numbers based on the plate length and the free-stream velocity at the plate leading edge were considered ($Re=70000, 150000, 220000$). The effects due to FST variation were investigated at $Re = 220000$ and $\alpha = 5$ degrees, since the boundary layer separates at the lower free-stream turbulence level for the other combinations of Re and pressure gradient. Overall, 10 flow conditions were examined concerning the systematic variation of all the aforementioned parameters (the flow conditions examined are summarized in table III).

B. Measuring techniques

The boundary layer evolving on the rear part of the plate was surveyed by means of a Dantec time-resolved PIV system (maximum repetition rate of 5 kHz). Two measurement planes were considered (see figure 1). The first measurement plane is aligned with the meridional section of the channel,

Statistical characterization of free-stream turbulence induced transition

4

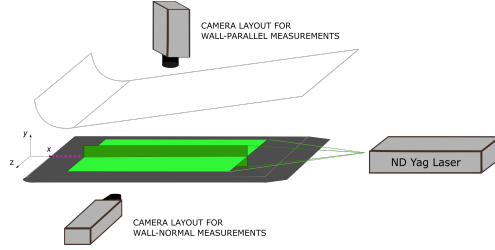


FIG. 1: Scheme of the test section and instrumentation layout (only the top surface is shown). Wall-normal and wall-parallel PIV measurement planes are depicted with green color. Pressure taps on the plate leading edge are highlighted with violet dots.

TABLE II: Turbulence-generating grids characterization: free-stream turbulence intensity (Tu), bars width (d), mesh size (M), and porosity parameter $\beta = (1 - d/M)^2$. Streamwise (L_x) and spanwise (L_z) integral length scales are reported.

| Grid | Re | Tu [%] | d [mm] | M [mm] | β | L_x [mm] | L_z [mm] |
|------|------|----------|----------|----------|---------|------------|------------|
| LTU | 70k | 2.5% | 2 | 8 | 0.64 | 11.5 | 3.2 |
| HTU | 70k | 3.5% | 4 | 8 | 0.36 | 13.1 | 4.6 |
| HHTU | 70k | 5% | 8 | 8 | 0 | 15.1 | 6.2 |
| LTU | 150k | 2.5% | 2 | 8 | 0.64 | 10.9 | 3.1 |
| HTU | 150k | 3.5% | 4 | 8 | 0.36 | 12.0 | 4.5 |
| HHTU | 150k | 5% | 8 | 8 | 0 | 14.3 | 6.1 |
| LTU | 220k | 2.5% | 2 | 8 | 0.64 | 10.3 | 2.8 |
| HTU | 220k | 3.5% | 4 | 8 | 0.36 | 11.1 | 4.2 |
| HHTU | 220k | 5% | 8 | 8 | 0 | 13.1 | 5.9 |

extending from the plate surface up to the free-stream region in the wall-normal direction (see Simoni et al.⁴²). The second one is oriented parallel to the plate surface, and it is embedded into the boundary layer (see the previous authors' work Dellacasagrande et al.⁴³). The extension of the wall-parallel plane in the spanwise direction was chosen in order to capture a sufficient number of alternating high- and low-speed streaks to compute their spanwise periodicity with a high level of accuracy. The streamwise position of the measuring domain was changed for the different cases in the region $0.3 < x/L < 1$, so that the entire transition process is captured for the different combinations of the flow parameters.

PIV measurements were performed by seeding the wind tunnel with vaseline oil droplets (mean diameter of $1.5 \mu m$), which were illuminated by a laser sheet with a 1 mm thickness. The instrumentation adopted is constituted by a dual-cavity Nd:YLF pulsed laser Litron LDY 300 (energy 30 mJ per pulse at 1000 Hz repetition rate, 527 nm wavelength). The light scattered by the seeding particles was recorded on a high sensitive SpeedSense M340 digital camera with a cooled 2560 x 1600 pixels CMOS matrix. For the present experiments, the magnification factor was set to about 0.16 for both measure-

TABLE III: Flow conditions examined: Reynolds number (Re), endwall opening angle (α), pressure gradient parameter ($k = \frac{v}{U_\infty} \frac{dU_\infty}{dx}$), free-stream turbulence intensity (Tu) and streamwise (L_x) and spanwise (L_z) integral length scales are reported.

| Re | α [deg] | k | Tu [%] | L_x [mm] | L_z [mm] |
|------|----------------|----------|----------|------------|------------|
| 150k | 12 | -3.9E-06 | 5 | 14.3 | 6.1 |
| 220k | 12 | -1.7E-06 | 5 | 13.1 | 5.9 |
| 70k | 9 | -6.3E-06 | 5 | 15.1 | 6.2 |
| 150k | 9 | -2.2E-06 | 5 | 14.3 | 6.1 |
| 220k | 9 | -1.3E-06 | 5 | 13.1 | 5.9 |
| 70k | 5 | -5.6E-06 | 5 | 15.1 | 6.2 |
| 150k | 5 | -1.3E-06 | 5 | 14.3 | 6.1 |
| 220k | 5 | -7.1E-07 | 5 | 13.1 | 5.9 |
| 220k | 5 | -7.1E-07 | 3.5 | 11.1 | 4.2 |
| 220k | 5 | -7.1E-07 | 2.5 | 10.3 | 2.8 |

ment planes. The adaptive cross-correlation was performed using a 16x16 pixels interrogation area with 50% overlap. This corresponds to a vector grid spacing of 0.43 mm, which ensures that boundary layer streaks are well resolved even for the highest Reynolds number. The relative error in the evaluation of the instantaneous velocity is expected to be smaller than 3.0% in the free-stream region, based on the analysis reported in Sciacchitano et al.⁴⁴ and Wieneke⁴⁵, and it grows to 6% in the boundary layer region for the wall-normal measurements (see also Dellacasagrande et al.⁴⁶). The detailed description of the experimental data and measuring techniques adopted in this work can be found in Verdoya et al.⁴⁷ and Simoni et al.⁴², where the possibility of using the present data base for the characterization and modeling of the boundary layer transition is discussed. For each condition, eight independent sets of 2000 instantaneous velocity fields were acquired at a sampling rate of 2 kHz in the wall-normal plane. Eight sets of 400 images were instead acquired in the wall-parallel plane with a lower sampling rate of 485 Hz, due to the larger field of view adopted in this case. With the PIV system operating in double frame mode, the time between laser pulses was chosen in order to achieve a particle displacement between the first and the second coupling snapshots of 1/4 of the interrogation region size. For the present cases, the delay time of the laser pulses was in the range 15 – 40 μs , depending on the flow Reynolds number. The large amount of PIV data collected were verified to allow the convergence of the statistical quantities obtained from both the measurement planes.

C. Data analysis

The time-averaged velocity distribution and the root mean square of velocity fluctuations were computed first for the statistical characterization of the boundary layer. Additionally, the instantaneous PIV snapshots collected in the wall-parallel plane were used to compute the streamwise and the spanwise wavelengths of boundary layer streaks. The intermittency function distribution was also computed for the different cases

based on a turbulent events recognition technique. To this end, the spatial root mean square (rms) of the spanwise fluctuating velocity component (w') computed over a cell of 5×5 measuring points was used as detection function (D) for turbulent events recognition:

$$D(x_k, z_m) = \sum_{i=k-2}^{k+2} \sum_{j=m-2}^{m+2} \sqrt{\frac{(w'(x_{k+i}, z_{m+j}) - \mu)^2}{25}} \quad (1)$$

where μ is the mean value of w' computed in each cell. The laminar flow is indeed dominated by velocity fluctuations aligned with the main direction of the flow since they are mainly due to the presence of ordered streaks (see e.g., Kreilos et al.³⁹). On the other hand, streak breakup leads to significant cross-flow fluctuations (see, e.g., Nolan and Zaki⁷, Kreilos et al.³⁹). Turbulent regions are therefore characterized by high values of the function D , whereas this latter is almost null in the laminar flow. Once D was computed for each PIV snapshot, its discrete laminar-turbulent representation was obtained based on the Otsu's method (Otsu³⁸). According to this procedure, the values of the function D are grouped in two distinct classes that are identified by minimization of the variance on each class. As specified in the work of Otsu³⁸, there are actually two options to find the threshold between classes. The first is to minimize the within-class variance, while the second is to maximize the between-class variance. Both options were verified to give the same result once applied to the present data sets. Then, since high values of the detection function D indicate the occurrence of turbulent events, D -values that are higher than the so derived threshold are classified as turbulent (and set equal to 1), whereas lower values are assumed to be related to laminar events and they are set equal to 0. The intermittency curve is then computed by means of integration along the spanwise coordinate and the temporal one of the binary maps of the detection function D (0-laminar, 1-turbulent). Figure 2 depicts the successive steps of this procedure. The top plot shows a PIV vector map of the perturbation velocity, where red and blue contoured regions of the streamwise fluctuating velocity highlight the presence of high- and low-speed streaks, respectively ($x/L < 0.6$). Downstream of $x/L = 0.6$, the presence of cross-flow fluctuations and wall-normal vorticity nuclei highlight the occurrence of breakup events. In the second plot, the contour of the detection function D is superimposed to the perturbation velocity vectors for the same PIV realization. The maximum values of D are detected for $x/L > 0.6$, where turbulent events occur. In the last plot, the discrete laminar-turbulent reduction of D obtained by means of the Otsu's method is given. Green contoured regions indicate turbulent portions of the boundary layer, while laminar ones are white contoured.

In this work, the probability density function of turbulent spot nucleation was computed for the entire data set. To this end, the binary maps obtained by means of the procedure previously described (see figure 2, bottom plot) are re-ordered along the statistically homogeneous spanwise direction following the same procedure described in the work of Nolan and Zaki⁷ for the analysis of DNS data. This directly provides the evolution of turbulent events from their inception to

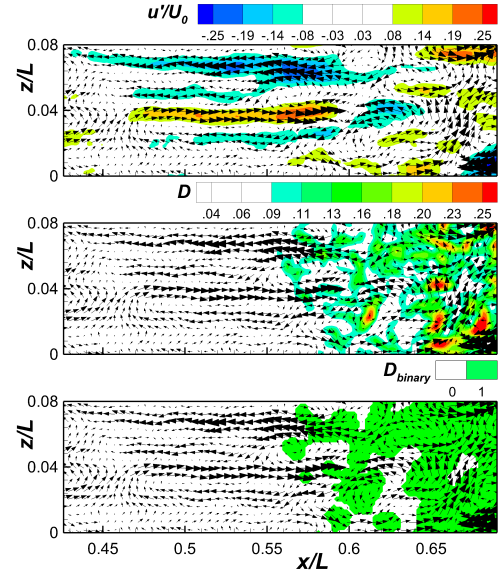


FIG. 2: Wall-parallel instantaneous PIV realization showing perturbation velocity vectors with superimposed the contour plot of (top) streamwise fluctuating velocity scaled with inlet free-stream velocity u'/U_0 , (middle) detection function D and (bottom) binarized contour plot of detection function D_{binary} . Streamwise and spanwise coordinates are scaled with the plate length L .

further downstream locations. More precisely, for each spanwise coordinate, the binarized values of the detection function D are plotted for the different streamwise positions as a function of the time instants at which they are computed. Figure 3 shows an example of such kind of representation for the present data set. The local maxima of the red line delimiting the turbulent (grey) and the laminar (white) regions are associated to the formation of new turbulent spots, which connect and merge at further streamwise positions and time instants. The present procedure therefore allows identifying the spatio-temporal locations at which spots are actually formed and to isolate nucleations from turbulent events that formed at upstream locations and are then convected downstream. The number of nucleation events (i.e. local maxima of the red line in figure 3) is then counted for all the streamwise locations to obtain the probability density function of spot nucleation for the different cases.

Since the streak scale plays an important role in the boundary layer transition, the streamwise and the spanwise scales of the streaky structures was computed for all the cases. The streamwise wavelength of unstable streaks showing sinuous motions was measured by means of visual inspection of the

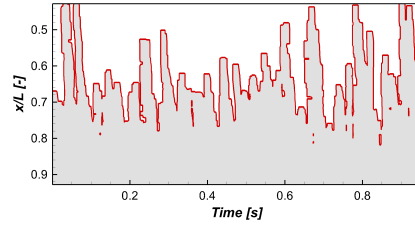


FIG. 3: Binary $x-t$ map for $z/L = 0$ (middle plate) obtained by means of Otsu's method. Grey and white contoured regions refer to turbulent and laminar flow, respectively. Streamwise coordinate is scaled with the plate length L .

PIV vector maps in both the measurement planes, by averaging over 30 independent samples for all cases (similar to what was done in Mans et al.²⁰). The spanwise scale of streaky structures was computed for each streamwise position by means of the spanwise auto-correlation function of the instantaneous streamwise velocity component (R_{uu}), following the same procedure adopted in the work of Matsubara and Alfredsson³.

III. TIME-AVERAGED FLOW DATA

The contour plots of the time-averaged streamwise velocity and the corresponding rms of velocity fluctuations are reported in figures 4-5 for four cases among the overall conditions, describing the effects due to Re , FST intensity and the pressure gradient on the time-averaged distribution of the boundary layer.

Figure 4 shows the contour plots of the time-averaged streamwise velocity scaled with the free-stream value U_0 measured at $x/L = 0.27$ and $y/L = 0.04$. Additionally, time-averaged velocity vectors are plotted at selected streamwise locations. In figure 4a the case $Re=70000-Tu=5\%-\alpha=9\text{deg}$ is shown, which is taken hereafter as reference. As a consequence of the adverse pressure gradient imposed to the flow, the boundary layer grows rapidly along the streamwise coordinate (see the black dashed line in the plot). Increasing the Reynolds number (figure 4b, $Re=220000$) makes the boundary layer thinner, and its streamwise growth rate is shown to change at about $x/L = 0.52$, suggesting that transition may occur around this position, as shown in the following sections. For the low pressure gradient (figure 4c) and the low FST (figure 4d) cases, the boundary layer shows constant growth for almost the entire PIV domain. In the following sections, the reduction of the adverse pressure gradient and FST intensity will be shown to delay the occurrence of breakup events, thus transition.

Figure 5 shows the rms of the streamwise velocity component scaled with the free-stream velocity U_0 for the same cases presented in figure 4. The maximum value of the rms profiles

is found close to the wall for all cases, as expected in the case of FST induced transition. Figure 5a shows the reference case. The increase and the successive reduction of the rms of velocity fluctuations suggest the occurrence of transition (see e.g., Matsubara and Alfredsson³). In figure 5b ($Re=220000$) the location where the maximum rms of velocity fluctuations occurs is shown to move upstream with respect to the previous case (compare figures 5a-b), whereas with the lower pressure gradient the highest rms values are observed further downstream (figure 5c). In the last plot of figure 5, the reduction of the FST intensity moves the maximum rms values downstream of $x/L = 0.6$.

Data shown in figures 4-5 were used for the computation of the main statistical quantities of the boundary layer, that can be used to characterize the boundary layer state at different streamwise positions. Figure 6 shows the streamwise variation of the intermittency function γ (black line) for the reference case. It is theoretically defined as the ratio between the time in which the flow is turbulent and the overall period of observation. As shown in the pioneering work of Narasimha et al.⁴⁸, the intermittency curve is a sigmoid function which is equal to 0 in the laminar BL and then reaches the unit value in the fully turbulent one. The maximum energy of streamwise fluctuations $(u'_{rms}/U_\infty)^2$ is also shown in figure 6, together with the shape factor (H_{12}) of the boundary layer. This latter is defined as the ratio between the displacement and the momentum thickness of the boundary layer. The comparison of these quantities allows discussing the link between the statistical parameters obtained from the wall-parallel (γ) and the wall-normal $((u'_{rms}/U_\infty)^2, H_{12})$ measuring plane. Transition is shown to start at about $x/L \approx 0.5$ and it ends at $x/L \approx 0.75$. The shape factor of the boundary layer decreases monotonically from the inlet to the outlet section of the measuring domain. Its value is about 2.5 where $\gamma = 0$ and then decreases to about 1.8 in the fully turbulent region, which is slightly higher than the value expected for fully turbulent boundary layer under zero pressure gradient. This deviation is ascribed to the strong adverse pressure gradient in the present experiments. The energy of streamwise fluctuations grows linearly up to about $x/L = 0.54$, then saturates and decreases as the boundary layer approaches the fully turbulent state (see Westin et al.¹ and Matsubara and Alfredsson³). The peak of $(u'_{rms}/U_\infty)^2$ occurs where $\gamma < 0.5$, which indicates that the higher streamwise fluctuations occur in the first half of transition region where ordered streaks are expected to dominate (in a statistical sense) with respect to breakup events. The trends discussed in figure 6 for the different quantities presented were observed for all the cases, but are not depicted here for brevity.

IV. INSTANTANEOUS FLOW DATA

In this work, time-resolved PIV realizations, such as those depicted in figure 7 (Multimedia view), were collected in the wall-normal and the wall-parallel planes for the statistical and the dynamical characterization of the coherent structures gov-

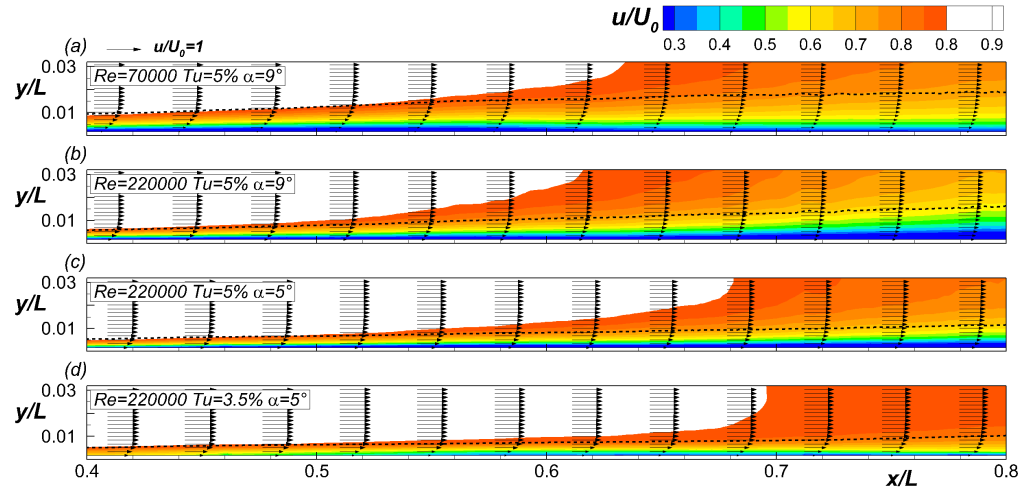


FIG. 4: Contour plots of time-averaged streamwise velocity: (a) $Re=70000$ - $Tu=5\%$ - $\alpha=9\text{deg}$, (b) $Re=220000$ - $Tu=5\%$ - $\alpha=9\text{deg}$, (c) $Re=220000$ - $Tu=5\%$ - $\alpha=5\text{deg}$, (d) $Re=220000$ - $Tu=3.5\%$ - $\alpha=5\text{deg}$. Data are scaled with the free-stream velocity U_0 measured at $x/L = 0.27$ and $y/L = 0.04$. Time-averaged boundary layer thickness is indicated with dashed black line. Time-averaged velocity vectors are reported. Streamwise and wall-normal coordinates are scaled with the plate length L .

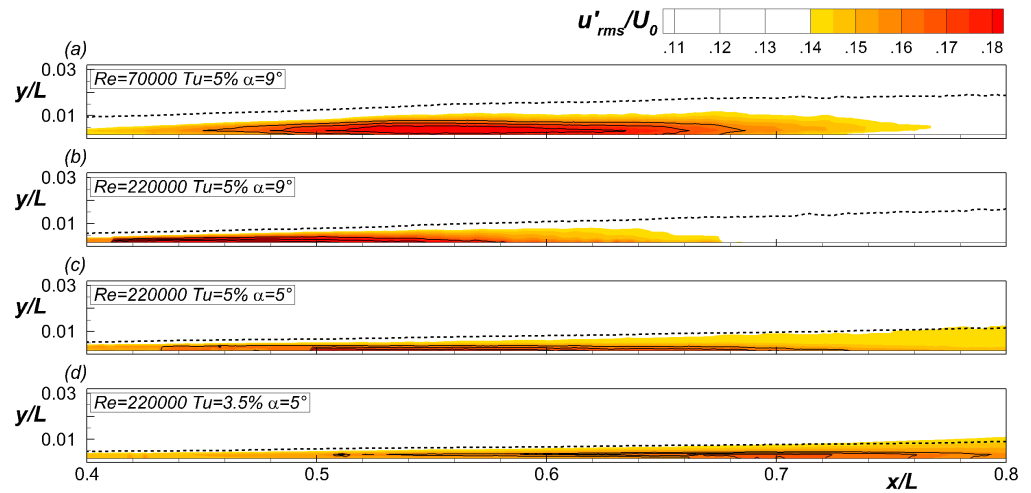


FIG. 5: Contour plots of root mean square of streamwise fluctuations: (a) $Re=70000$ - $Tu=5\%$ - $\alpha=9\text{deg}$, (b) $Re=220000$ - $Tu=5\%$ - $\alpha=9\text{deg}$, (c) $Re=220000$ - $Tu=5\%$ - $\alpha=5\text{deg}$, (d) $Re=220000$ - $Tu=3.5\%$ - $\alpha=5\text{deg}$. Data are scaled with the free-stream velocity U_0 measured at $x/L = 0.27$ and $y/L = 0.04$. Time-averaged boundary layer thickness is indicated with dashed black line. Contour lines of $u'_{rms}/U_0 = 0.16, 0.17$ and 0.18 are added to the plots. Streamwise and wall-normal coordinates are scaled with the plate length L .

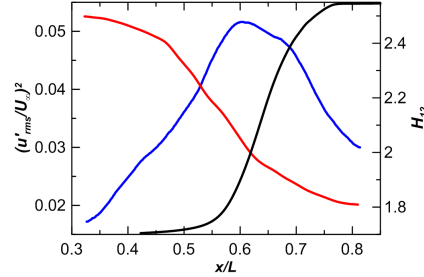


FIG. 6: Streamwise variation of (—) energy of streamwise fluctuations scaled with local free-stream velocity $(u'_{rms}/U_\infty)^2$, (—) shape factor H_{12} and (—) intermittency function γ (ranging between 0 and 1 in the plot).

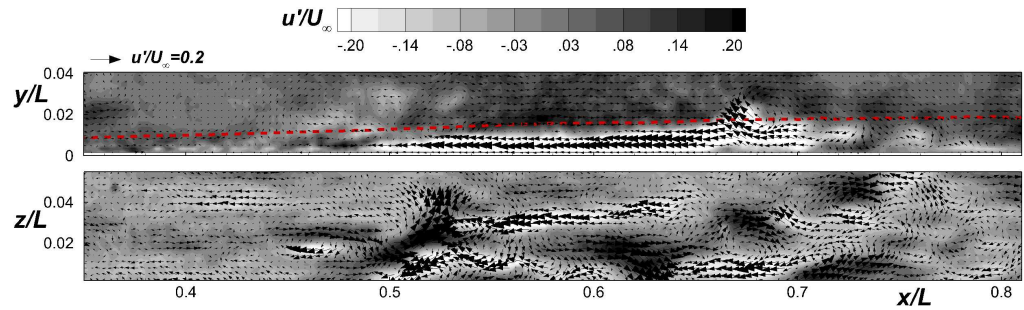


FIG. 7: Instantaneous perturbation velocity vectors obtained by the classical Reynolds decomposition superimposed to the contour plot of u'/U_∞ collected in (top) the wall-normal and (bottom) the wall-parallel plane. Data refer to the case $Re=70000-Tu=5\%-\alpha=9\text{deg}$. Time-averaged boundary layer thickness is indicated with dashed red line in the wall-normal frame. Coordinates are scaled with plate length L . The number of depicted velocity vectors is reduced to increase the readability of the plot (Multimedia view).

erning the transition process of the boundary layer.

A. Wall-normal plane data

Figures 8-11 show sequences of PIV realizations collected in the wall-normal plane for the same cases presented in figures 4-5, which directly provide a qualitative view of streak dynamics for different values of the Reynolds number, FST intensity and the adverse pressure gradient. To better isolate ordered streaks and breakup events embedded within the flow, the snapshots presented herein are filtered by means of Proper Orthogonal Decomposition⁴⁹. Moreover, the contour plot of the streamwise fluctuations is superimposed to the vector maps of the instantaneous fluctuating velocity, to highlight the occurrence of high- and low-speed streaks.

Figure 8 shows three PIV realizations for the reference case $Re=70000-Tu=5\%-\alpha=9\text{deg}$. The top plot shows a low-speed streak close to the edge of the boundary layer for $x/L < 0.55$,

with Q_2 events (i.e. *ejections*, $u' < 0$ and $v' > 0$, see e.g., Nolan et al.⁵⁰, Nolan and Walsh²⁹) occurring near this position (see the blue circle at about $x/L = 0.565$). In the successive realizations, the streak exhibits wall-normal motions. In the second and the third plots, ejections are strengthened and vortical structures (blue circles) are observed at $x/L = 0.55$ and $x/L = 0.59$, resembling the signatures of hairpin vortices in this plane (see e.g., Adrian⁵¹). Downstream of $x/L = 0.65$, finer scale structures occurring randomly can be observed and the streak is almost completely disrupted. Note that this is the position corresponding to $\gamma \approx 0.5$ (see figure 6), where most of spot nucleations were found to occur, as discussed in the following sections.

Figure 9 shows three PIV realizations for the case $Re=220000-Tu=5\%-\alpha=9\text{deg}$. Note that the PIV snapshots are plotted here for $0.39 < x/L < 0.65$, since the field of view was centered on the maximum value of the rms of the streamwise velocity (figure 5b). A low-speed streak can be observed in the first plot of figure 9 for $x/L < 0.5$, which is thinner than

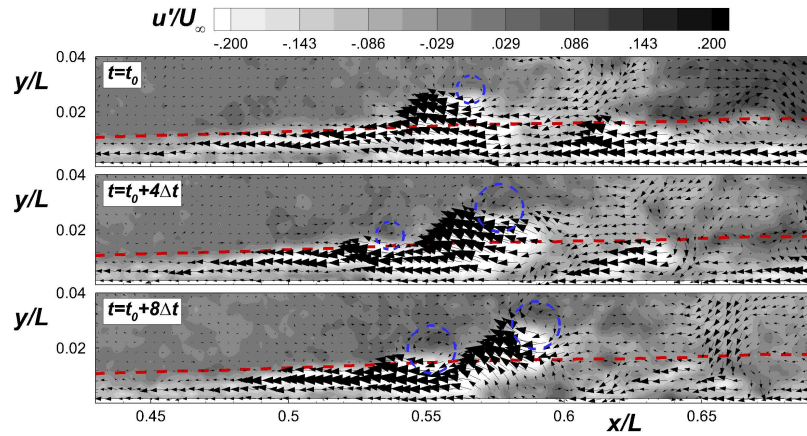


FIG. 8: Instantaneous perturbation velocity vectors obtained by the classical Reynolds decomposition superimposed to the contour plot of u'/U_∞ collected in wall-normal plane. Data refer to the case $Re=70000$ - $Tu=5\%$ - $\alpha=9\text{deg}$. Time-averaged boundary layer thickness is indicated with dashed red line. Streamwise and wall-normal coordinates are scaled with plate length L . The number of depicted velocity vectors is reduced to increase the readability of the plots.

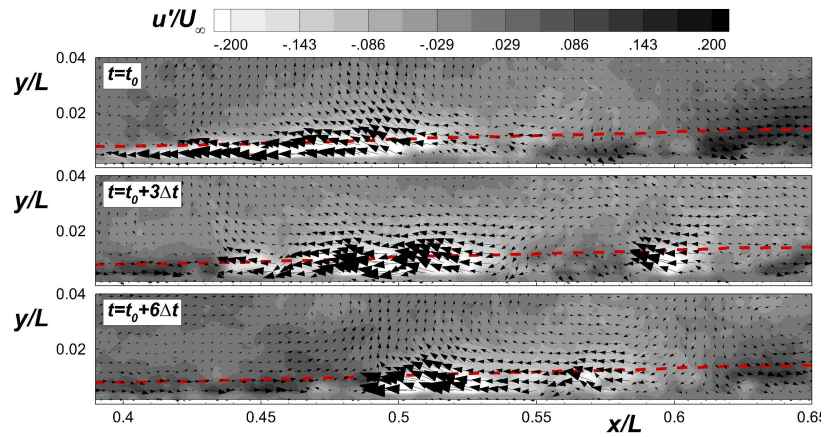


FIG. 9: Instantaneous perturbation velocity vectors obtained by the classical Reynolds decomposition superimposed to the contour plot of u'/U_∞ collected in wall-normal plane. Data refer to the case $Re=220000$ - $Tu=5\%$ - $\alpha=9\text{deg}$. Time-averaged boundary layer thickness is indicated with dashed red line. Streamwise and wall-normal coordinates are scaled with plate length L . The number of depicted velocity vectors is reduced to increase the readability of the plots.

that observed for the low Re case (figure 8) and it is more confined toward the wall. This is ascribed to the change of the time-averaged structure of the boundary layer (i.e. the base flow) due to Reynolds number variation since the other parameters are kept the same as in figure 8. At $x/L = 0.48$,

Q_2 events occur in the first plot, while in the successive ones the low speed streak exhibits wave-like motion preluding to streak breakup. Wall-normal fluctuations and streak breakup are shown to occur upstream with respect to the low Re case,

This is the author's peer reviewed, accepted manuscript. However, the online version of record will be different from this version once it has been copyedited and typeset.

PLEASE CITE THIS ARTICLE AS DOI: 10.1063/1.50063948

Statistical characterization of free-stream turbulence induced transition

10

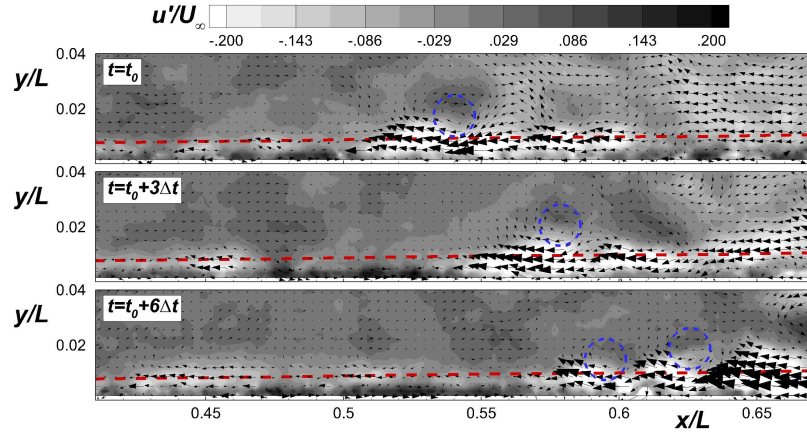


FIG. 10: Instantaneous perturbation velocity vectors obtained by the classical Reynolds decomposition superimposed to the contour plot of u'/U_∞ collected in wall-normal plane. Data refer to the case $Re=220000-Tu=5\%-\alpha=5\text{deg}$. Time-averaged boundary layer thickness is indicated with dashed red line. Streamwise and wall-normal coordinates are scaled with plate length L . The number of depicted velocity vectors is reduced to increase the readability of the plots.

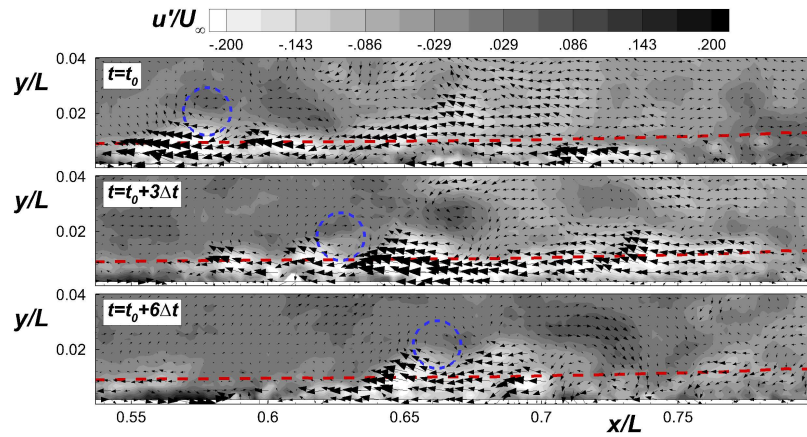


FIG. 11: Instantaneous perturbation velocity vectors obtained by the classical Reynolds decomposition superimposed to the contour plot of u'/U_∞ collected in wall-normal plane. Data refer to the case $Re=220000-Tu=3.5\%-\alpha=5\text{deg}$. Time-averaged boundary layer thickness is indicated with dashed red line. Streamwise and wall-normal coordinates are scaled with plate length L . The number of depicted velocity vectors is reduced to increase the readability of the plots.

thus an earlier transition is expected to take place. PIV snapshots for the case $Re=220000-Tu=5\%-\alpha=5\text{deg}$ are presented in figure 10, to highlight the effects due to the pressure gradient variation by comparison with figure 9. A low speed streak can be observed in the first plot for $x/L < 0.6$, where

Q_2 events with spanwise oriented vortices (blue circles) occur. In the third snapshot the signature of hairpin vortices and the associated ejection events are clearly observable for $x/L > 0.6$. Comparing figures 9 and 10, one can clearly see that the breakup of the detected streak occurs further down-

This is the author's peer reviewed, accepted manuscript. However, the online version of record will be different from this version once it has been copyedited and typeset.

PLEASE CITE THIS ARTICLE AS DOI: 10.1063/5.0063948

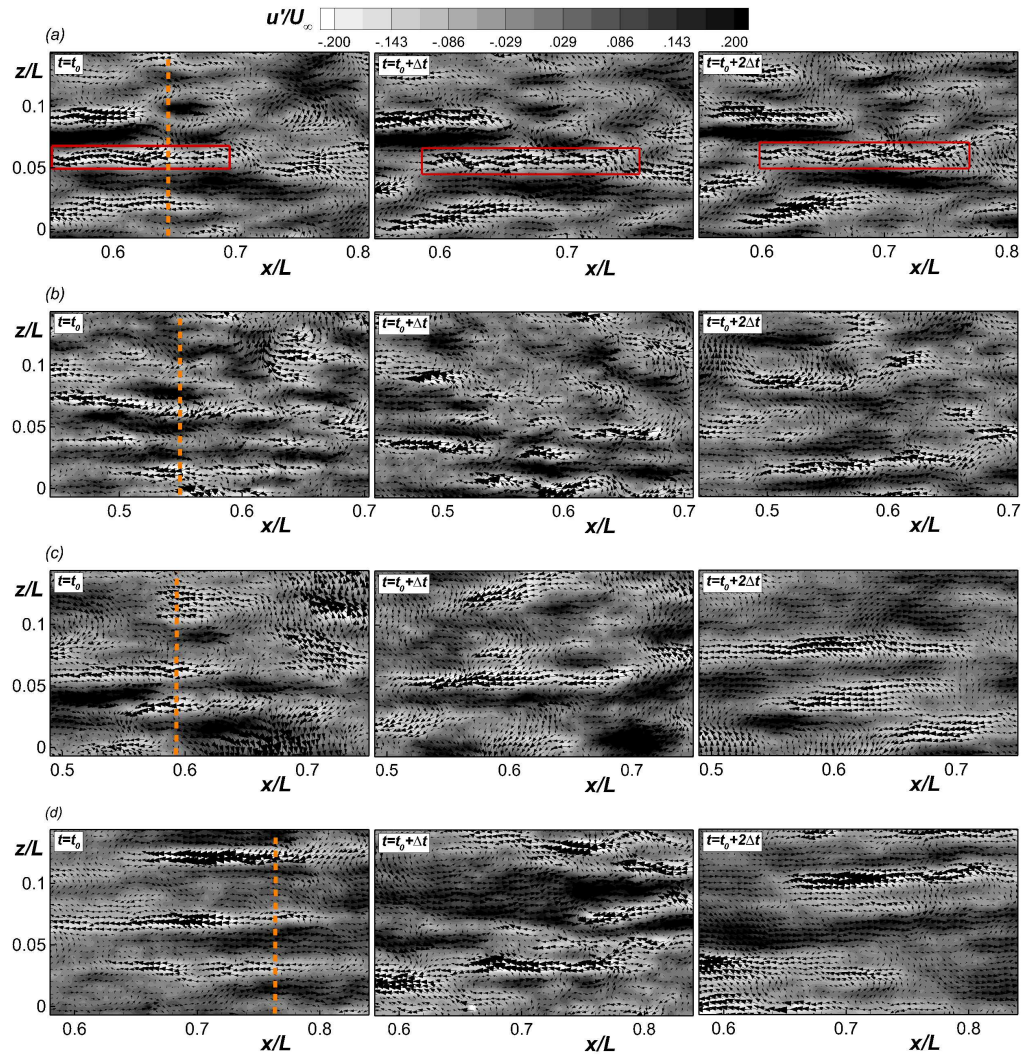


FIG. 12: Instantaneous perturbation velocity vectors obtained by the classical Reynolds decomposition superimposed to the contour plot of u'/U_∞ collected in wall-parallel plane: (a) $Re=70000-Tu=5\%-\alpha=9\text{deg}$, (b) $Re=220000-Tu=5\%-\alpha=9\text{deg}$, (c) $Re=220000-Tu=5\%-\alpha=5\text{deg}$, (d) $Re=220000-Tu=3.5\%-\alpha=5\text{deg}$. Streamwise and spanwise coordinates are scaled with plate length L . The number of depicted velocity vectors is reduced to increase the readability of the plots. The position of mid-transition (i.e. where $\gamma = 0.5$) is indicated with vertical dashed line in the first plot of each sequence. The streamwise range shown in the plots is different for the cases presented according to the different locations at which breakup events occur.

stream reducing the adverse pressure gradient, as it will be discussed in details in the following sections. Finally, the comparison between figures 10 and 11 provides the effects due to the turbulence intensity variation. In figure 11 the free-stream turbulence is reduced from 5% to 3.5% and data are plotted for different streamwise positions due to the significant spatial shift required for detecting breakup events. For the present case, the PIV realizations show a low speed streak at about $0.56 < x/L < 0.65$ (first plot), which becomes rapidly unstable in the successive realizations. The signatures of hair-pin vortices are also observed in this case in the second and the third plots for $x/L > 0.62$, thus reducing the free-stream turbulence delays the occurrence of breakup events.

B. Wall-parallel plane data

PIV realizations performed in the wall-parallel plane for the same cases shown in figures 8-11 are presented in figure 12 to highlight the occurrence of alternating high- and low-speed streaks in the boundary layer. Note that since full-frame realizations are depicted here, which were acquired at a lower sampling frequency due to the limitations of the PIV system adopted, time-resolved observations are provided only for the low Re cases. The sampling period in this plane is $\Delta t = 0.0021\text{sec}$, which is higher than that adopted in the wall-normal one ($\Delta t = 0.0005\text{sec}$). Additionally, to better highlight the region of breakup events, the position corresponding to $\gamma = 0.5$ is indicated with vertical dashed line in the first plot of each snapshot sequence.

The reference case $Re=70000-Tu=5\%-\alpha=9\text{deg}$ is reported in figure 12a. The first PIV realization of figure 12a shows ordered streaks for $x/L \leq 0.65$, according to the intermittency function distribution shown in figure 6. Note that sinuous motions of boundary layer streaks are recognizable in the PIV snapshots (see the low-speed streak in the red box). Then, normal to the wall vorticity nuclei and turbulent events with smaller scale are observed for $x/L > 0.68$, according to what was observed in the wall-normal plane (see figure 8).

In figures 12b-d the effects due to Re , pressure gradient and FST intensity variation are presented. Figure 12b shows three PIV realizations for the case $Re=220000-Tu=5\%-\alpha=9\text{deg}$. Comparing figure 12b with figure 12a, boundary layer streaks are evidently thinner and shorter, due to the reduction of the boundary layer thickness, as previously observed in figure 4. For the present case, breakup events are shown to occur just downstream of $x/L > 0.55$, where spanwise fluctuations increase significantly. Figure 12c shows the case $Re=220000-Tu=5\%-\alpha=5\text{deg}$, highlighting the effects due to the pressure gradient variation by comparison with figure 12b. Cross-flow fluctuations originating from breakup events are mostly detected downstream of $x/L = 0.6$, which indicates that streak instability is delayed at lower adverse pressure gradient (see also figure 10). Similar effects are observed as a consequence of the reduction of the free-stream turbulence intensity. Figure 12d shows PIV realizations for the case $Re=220000-Tu=3.5\%-\alpha=5\text{deg}$. Ordered streaks are observed up to about

$x/L = 0.75$. Downstream of this position, smaller structures are observed as a consequence of streak breakup.

V. STREAMWISE AND SPANWISE SCALE OF STREAKY STRUCTURES

The PIV data collected in the wall-parallel plane are used in this work for the computation of the spanwise and the streamwise wavelength of streaky structures, from the laminar to the turbulent region of the boundary layer. The aim is to provide the characterization, in a statistical sense, of the effects due to Re , FST intensity and pressure gradient variation on the main structures driving the transition process. Figures 13a and 13b show the streamwise variation of the minimum of the spanwise correlation function of streamwise fluctuations (Δz_{min}), which corresponds to half of the spanwise wavelength of streaky structures, as discussed in the previous literature work of Matsubara and Alfredsson³. The curves depicted in figures 13a and 13b are scaled with the local displacement (δ^*) and momentum (θ) thickness, respectively, to highlight the link between the streak scale and the local boundary layer dimension.

The results presented in figure 13a extend the findings of the previous literature work of Matsubara and Alfredsson³ for zero pressure gradient. In the laminar region, the streak spacing is significantly larger than the displacement thickness of the boundary layer. The greatest effects due to the modification of the flow parameters are shown in the fore part of the plate for $x/L < 0.5$. The quantity $\Delta z_{min}/\delta^*$ is shown to increase in this portion of the plate when increasing the Reynolds number as well as reducing both the pressure gradient and the free-stream turbulence. Particularly, the higher values of the dimensionless streak spacing are observed for the lowest diffusion and the lowest free-stream turbulence level at high Reynolds number. The parameters considered herein have been shown to affect the mean structure of the laminar boundary layer, thus modifying the ratio between the spanwise length scale of streaky structures and the boundary layer dimension. Otherwise, the dimensional streak spacing was found to be only slightly affected by Re and the pressure gradient. Moving towards the end of the PIV domain, $\Delta z_{min}/\delta^*$ reduces monotonically for all the cases, and the curves collapse to a value of about 3 for $x/L > 0.65$. This indicates that, at a certain streamwise location, the boundary layer dimension and the spanwise scale of streaky structures are about the same, regardless of the Reynolds number, FST intensity and pressure gradient. The present results therefore highlight how the streak scale matches the boundary layer thickness even under strong adverse pressure gradient for different Reynolds numbers and turbulence intensity levels. It should be noted here that reducing both the pressure gradient and the FST intensity, the quantity $\Delta z_{min}/\delta^*$ reaches the asymptotic value far downstream with respect to the other cases. The PIV snapshots reported in figures 10-12 showed that breakup events are delayed for the lower FST intensity and pressure gradient conditions, as further discussed in the following. Therefore, the present results suggest that the lo-

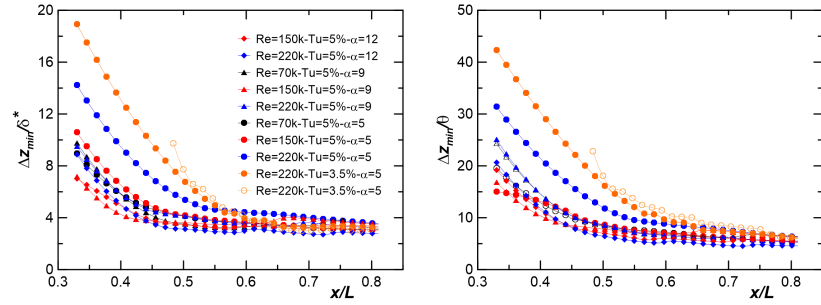


FIG. 13: Streamwise variation of spanwise distance between high- and low-speed streaky structures obtained from the spanwise auto-correlation function of PIV snapshots. Streak spacing is scaled with (left) the local displacement thickness and (right) the local momentum thickness of the boundary layer. Conditions are labeled with the corresponding values of Re , Tu level and opening angle of the channel ($\alpha=12, 9, 5$ degrees).

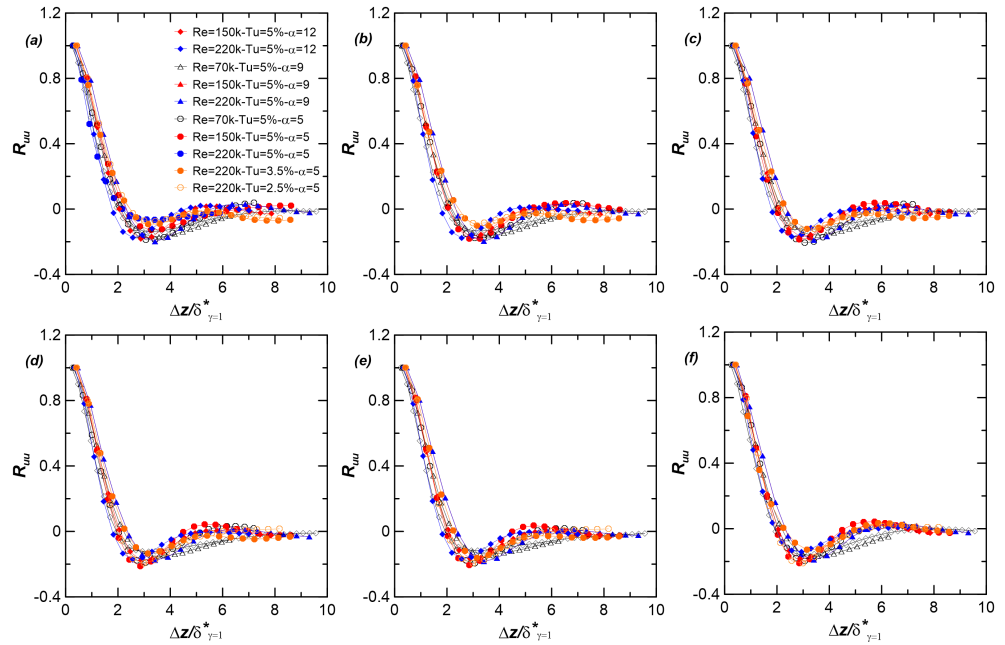


FIG. 14: Spanwise correlation function of streamwise velocity computed from PIV data at the locations where (a) $\gamma = 0.1$, (b) $\gamma = 0.2$, (c) $\gamma = 0.3$, (d) $\gamma = 0.4$, (e) $\gamma = 0.5$, (f) $\max(u'_{rms})$. The spanwise coordinate is scaled with the displacement thickness computed at the location where $\gamma = 1$ ($\delta_{\gamma=1}^*$). Conditions are labeled with the corresponding values of Re , Tu level and opening angle of the channel ($\alpha=5, 9, 12$ degrees).

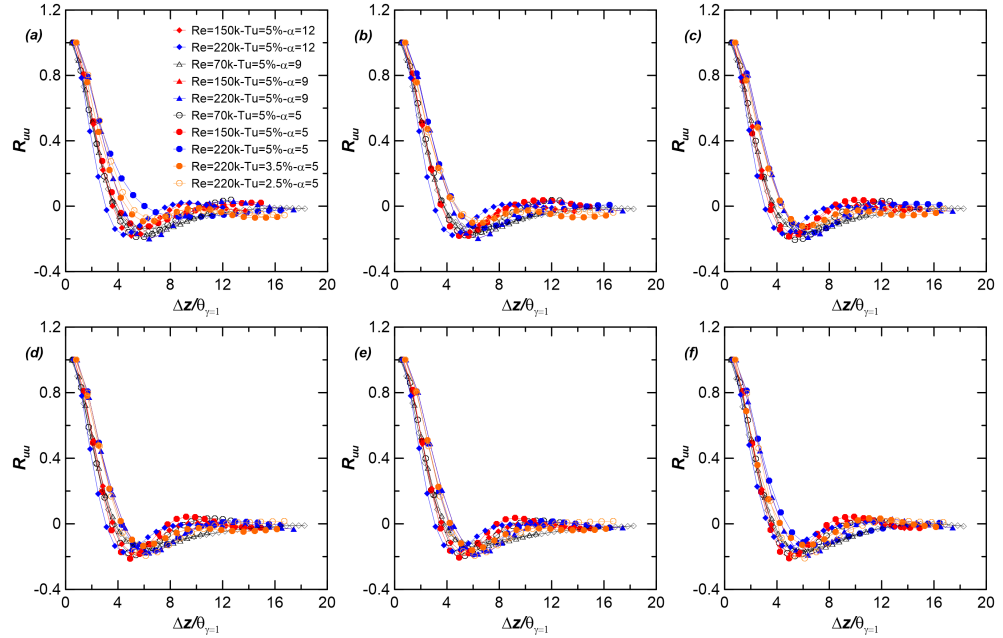


FIG. 15: Spanwise correlation functions of streamwise velocity computed from PIV data at the locations where (a) $\gamma = 0.1$, (b) $\gamma = 0.2$, (c) $\gamma = 0.3$, (d) $\gamma = 0.4$, (e) $\gamma = 0.5$, (f) $\max(u'_{rms})$. The spanwise coordinate is scaled with the momentum thickness computed at the location where $\gamma = 1$ ($\theta_{\gamma=1}$). Conditions are labeled with the corresponding values of Re , Tu level and opening angle of the channel ($\alpha=12, 9, 5$ degrees).

tion where streak breakup occurs may be linked to the local boundary layer scale compared to the streak spacing. The curves shown in figure 13b ($\Delta z_{min}/\theta$) show the same trend of those depicted in figure 13a, but they converge to a value of about 5 at the end of the PIV domain. Moreover, the effects due to the flow parameter variation are substantially the same. As a consequence, both δ^* and θ can be used as scaling quantities for the streak spacing.

The superposition of all the curves depicted in figure 13 in the rear part of the plate, where breakup events were shown to occur (see figures 8-12), indicates that the integral parameters of the turbulent boundary layer scale well the spanwise wavelength of boundary layer streaks. Alternatively, from a different perspective, the mean structure of the turbulent boundary layer is strongly linked to the streak dimension. In order to better investigate the similarity properties of streaky structures in the transition region, as well as their link to the time-averaged structure of the turbulent boundary layer, the dimensionless streak spacing has been compared for the different cases at fixed positions along the transition process (i.e. for the same value of the intermittency function). Figures 14 and 15 show the spanwise auto-correlation function of streamwise fluctuations (R_{uu}) for $\gamma = (0.1, 0.2, 0.3, 0.4, 0.5)$, with the tur-

bulent displacement and momentum thickness used as scaling quantities (indicated as $\delta^*_{\gamma=1}$ and $\theta_{\gamma=1}$, respectively). The comparison at the location of the absolute maximum u'_{rms} is also shown. Interestingly, the minimum of the correlation function collapses for all the cases in the transition region once it is scaled with the turbulent values of both δ^* and θ , regardless of the Re , FST intensity and the pressure gradient. The spanwise periodicity of the boundary layer streaks, which formed far upstream in the laminar region, and the time-averaged structure of the turbulent boundary layer are therefore strictly linked.

For a complete characterization of the streak wavelengths and their link to the mean boundary layer structure, the streamwise wavelength of unstable streaks was also measured by means of visual inspection of the PIV realizations (similar to the work of Mans et al.²⁰), such as those reported in figures 8-12. More precisely, boundary layer streaks showing sinuous breakup were detected (see e.g. figure 12a). The corresponding streamwise wavelength was measured for each case and it was averaged over 30 independent samples. The streamwise wavelength of streaky structures was scaled with the displacement thickness of the boundary layer computed at the position where sinuous instability starts to occur. The

quantity λ_x/δ^* was found to be in the range $9.7 \div 14.5$ for all the Reynolds numbers, FST intensity and pressure gradients. This is in good agreement with the previous literature works of Brandt et al.⁵², Mans et al.²⁰ and Schlatter et al.¹⁹ for instance, where the streamwise wavelength of unstable streaks was found to be in the range 12-28 under zero pressure gradient conditions and with different values of FST intensity. Therefore, the present analysis indicates that the quantity λ_x/δ^* is only slightly affected by the variation of pressure gradient and Reynolds number, other than the FST.

VI. TURBULENT SPOT NUCLEATION

Figure 16 shows the PDFs of spot nucleation computed as described in section II C together with the intermittency function distribution for different values of the Reynolds number, Tu level and the adverse pressure gradient. Histograms are computed in such a way that the sum of the bin values is equal to 1. Some cases among the overall tested conditions are shown here to present the effects due to the variation of these parameters. It should be pointed out that due to the reduced thickness of the BL at the beginning of transition (especially at higher Reynolds numbers), the accuracy in the recognition of turbulent spots nucleation is lower than at further downstream locations. For this reason, nucleation events in the region where $\gamma < 0.05$ (i.e. where a small number of turbulent events occurs) are neglected during the computation of the PDF. The results presented here show that the region of maximum spot inception is affected by the flow parameters variation. Additionally, the PDF peaks move with respect to the transition onset location, as shown by comparison with the corresponding intermittency curves.

At fixed pressure gradient and FST intensity, the location where the maximum number of nucleation events occur moves upstream as the Reynolds number increases (top plots of figure 16, Re increases from left to right). Similar effects can be observed increasing the adverse pressure gradient at fixed Reynolds number and FST intensity (middle plots of figure 16, APG increases from left to right). Under stronger adverse pressure gradient, the region of maximum spot nucleations moves slightly upstream. The smaller effects due to APG variation on the location where transition occurs seem in good agreement with the observations reported in Abu-Ghannam and Shaw⁵³. The authors showed that the Reynolds number based on the momentum thickness at the transition onset position is unaffected by the pressure gradient variation for Tu level higher than about 3.5% (as for the present cases). Otherwise, the standard deviation of the PDF reduces significantly (see table IV) and the transition region is shortened when the APG increases (see also Nolan and Zaki⁷). Interestingly, the PDFs of nucleation events exhibit right skewness when increasing both the Reynolds number and especially the APG, indicating that most of the turbulent spots start to form in a narrow streamwise window, while their production sensibly decreases at further downstream positions.

The bottom plots of figure 16 show the effects due to the modification of FST intensity (Tu level increases from left

to right). The location corresponding to the highest number of spot nucleations moves upstream as the free-stream turbulence increases. Moreover, for $Tu=2.5\%$ and 3.5% , the highest number of spot nucleations occurs where $\gamma < 0.3$ (with the PDF being right-skewed), thus breakup events are confined in a narrow portion of the transition region. On the contrary, for $Tu=5\%$ the peak of the PDF occurs around the location of mid-transition (i.e. where $\gamma \approx 0.5$) and the standard deviation of the PDF sensibly increases (bottom-right plot). In this sense, the free-stream turbulence intensity is the parameter showing the greatest effect on the PDF variance among those tested here (see table IV). Brandt and De Lange²² showed that under high level of free-stream turbulence, many streaks are formed randomly in space and time and their interaction, which occurs randomly as well, plays an important role in the occurrence of breakup events. This is the reason why at the highest Tu level, spot nucleation events are observed to occur in a wider streamwise window with respect to the lower free-stream turbulence cases, indicating that streak breakup occurs more randomly in space. Additionally, it should be noted that for the cases with $Tu=5\%$, the transition length increases (i.e. the slope of the intermittency function reduces). Similar behavior was found in the work of Fransson et al.⁶ for flat plate boundary layer, where the transition length was found to increase with increasing the FST intensity above 2.5%.

With the aim of analysing the similarity properties of the PDFs presented here, they were plotted in terms of a newly defined variable which takes into account of the effects due to all the flow parameters tested in this work. In section V, the ratio between the local streak spacing and the momentum thickness of the boundary layer was shown to converge to a fixed value moving toward the transition region, where nucleation events occur. In this sense, the dimensionless streak wavelength λ_c/θ (which is directly linked to the quantity $\Delta z_{min}/\theta$ shown in figure 13) is supposed to be a good ingredient for the definition of a proper scaling quantity for the PDF of nucleation events. Moreover, the location where the maximum number of nucleations occurs, as well as the standard deviation of the corresponding PDFs, were shown to be affected by the Reynolds number and the pressure gradient. Both these two parameters affect the streamwise growth and the time-averaged structure of the boundary layer. For this reason, the shape factor of the boundary layer H_{12} is also considered for scaling the PDF distributions reported in figure 16. Then, in order to account for the relevant effects due to Tu level variation highlighted in figure 16, this quantity has been also introduced in the definition of a non-dimensional abscissa (\hat{x}_{PDF}), defined as:

$$\hat{x}_{PDF} = \frac{\lambda_c}{\theta} H_{12} Tu \quad (2)$$

which can be also recast into the following expression:

$$\hat{x}_{PDF} = \frac{\lambda_c u'_{rms}}{v} \frac{v}{U_\infty} H_{12} = \frac{Re_{\lambda_c}}{Re_\theta} H_{12} \quad (3)$$

Thus, the non-dimensional abscissa defined in equations (2)-(3) can be equivalently seen as a combination of a perturbation based Reynolds number (Re_{λ_c}) and the momentum thick-

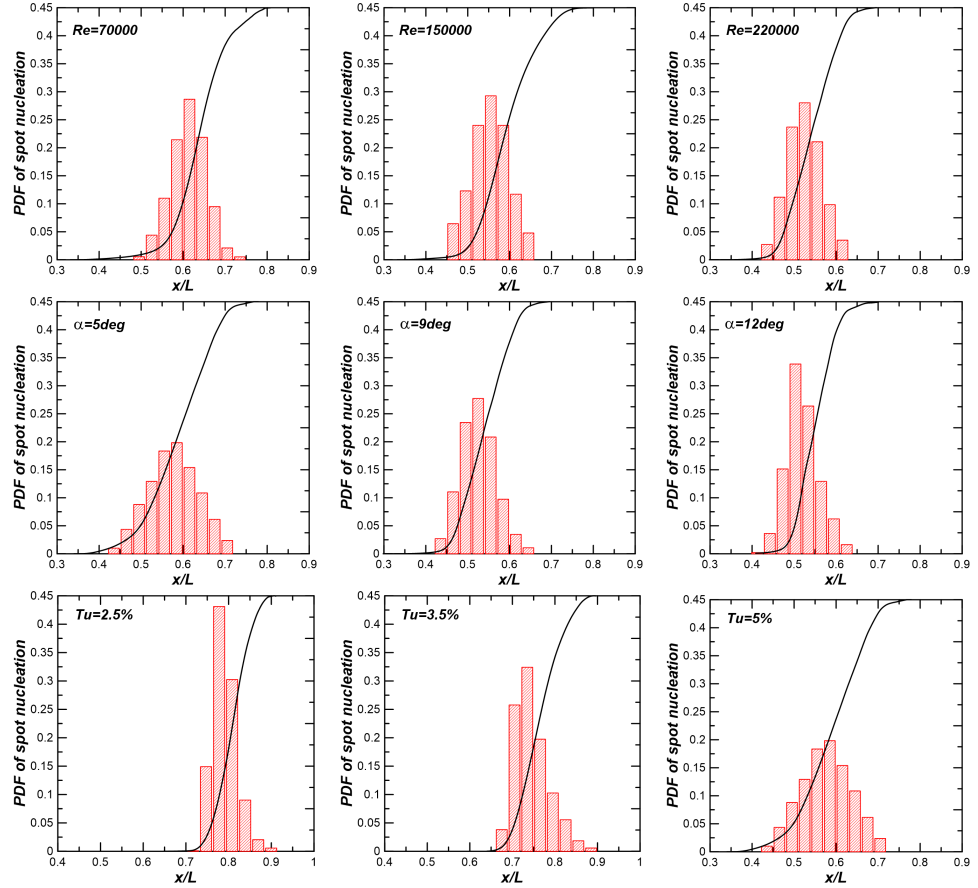


FIG. 16: Probability density function of turbulent spot nucleation with intermimty function (rangib between 0 and 1 in the plots). Top plots form left to right: $Re=70000-Tu=5\%-\alpha=9deg$, $Re=150000-Tu=5\%-\alpha=9deg$, $Re=220000-Tu=5\%-\alpha=9deg$. Middle plots from left to right: $Re=220000-Tu=5\%-\alpha=5deg$, $Re=220000-Tu=5\%-\alpha=9deg$, $Re=220000-Tu=5\%-\alpha=12deg$. Bottom plots from left to right: $Re=220000-Tu=2.5\%-\alpha=5deg$, $Re=220000-Tu=3.5\%-\alpha=5deg$, $Re=220000-Tu=5\%-\alpha=5deg$.

ness Reynolds number (Re_θ). Additionally, the term Re_{λ_c} appearing in equation 3 can be also linked to the FST Reynolds number introduced in the recent work of Fransson and Shahinfar⁸, where the streak spacing was found to be linked to the FST characteristics. Figure 17 shows the normalized PDFs computed for all the cases plotted as a function of the mixed variable defined in equation (2). Note that the quantity \hat{x}_{PDF} is monotonically decreasing, so the flow direction in figure 17 is from the right to the left of the plot. Interestingly, the PDFs are shown to collapse one to each other, in terms of both the maximum peak location and their standard deviation, with a good level of approximation (the higher dispersion is

observed at the beginning of transition). Turbulent spots are shown to form between $\hat{x}_{PDF} \approx 60$ and 200, with the maximum peak of the scaled PDFs occurring at about $\hat{x}_{PDF} \approx 100$. The parameters used for the definition of the scaling quantity reported in equation 2 are therefore considered to capture the response of turbulent spot nucleation to the variation of the external forcing (i.e Tu level), and to the modification of the boundary layer structure due to either the Reynolds number and the adverse pressure gradient variation.

In figure 17, the parametric function previously defined in the work of Kreilos et al.³⁹ for the prediction of the stream-

TABLE IV: Standard deviation of PDF of nucleation events expressed in terms of x/L .

| $Re - Tu$ | 70000-5% | 150000-5% | 220000-5% | 220000-3.5% | 220000-2.5% |
|------------------|----------|-----------|-----------|-------------|-------------|
| $\alpha = 12deg$ | - | 0.036 | 0.033 | - | - |
| $\alpha = 9deg$ | 0.042 | 0.040 | 0.035 | - | - |
| $\alpha = 5deg$ | 0.051 | 0.048 | 0.046 | 0.032 | 0.027 |

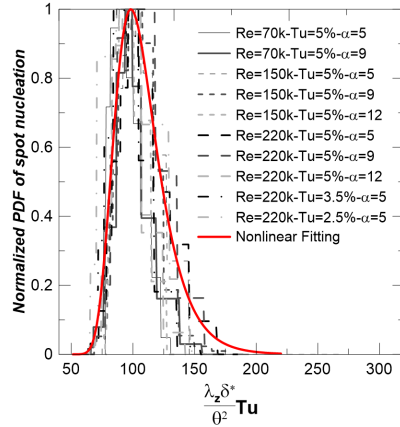


FIG. 17: Normalized PDFs of spot nucleations for all Reynolds numbers, Tu levels and pressure gradients plotted as a function of the non-dimensional abscissa $x_{PDF} = \frac{\lambda_x \delta^+}{\theta^2} Tu$. Conditions are labeled with the corresponding values of Re , Tu level and opening angle of the channel ($\alpha=12, 9, 5$ degrees). Fitting curve obtained by means of non-linear fit to the data is also plotted with solid red line.

wise variation of the spot nucleation rate:

$$p_c(x) = \frac{\lambda(r-1)A_E}{\sqrt{\pi}\sigma} e^{\left(-\frac{1+(r-1)e^{-\lambda x}}{\sigma A_E}\right)^2} e^{-\lambda x} \quad (4)$$

is also shown (red line), where the coefficient values $r = 1.23$, $\sigma = 0.0375$ and $\lambda = 0.117$ are obtained here by means of non-linear fit to the normalized PDFs obtained from the present experiments (with A_E set equal to 1 as in Kreilos et al.³⁹). It is pointed out here that the coefficient values providing the minimum mean squared error strongly depend on the coordinate adopted and the quantity to be fitted. The coefficient values obtained from the present fitting procedure are therefore significantly different to those obtained by Kreilos et al.³⁹ ($r = 145$, $\sigma = 1.05$ and $\lambda = 0.017$), where the effects due to only the Tu level variation were considered. However, it is worth noticing that the functional shape previously provided in the work of Kreilos et al.³⁹ is able to mimic the overall behavior of the scaled PDFs computed in this work. This indicates that further investigations concerning the response of the fitting coefficients to Reynolds number, pressure gradient and

Tu level variation should be carried out considering a wider range of flow conditions.

VII. CONCLUSIONS

The free-stream turbulence induced transition of a flat plate boundary layer has been studied using time-resolved particle image velocimetry under variable Reynolds number, Tu level and adverse pressure gradient. The statistical characterization of the BL structures and the overall transition process has been provided in terms of the mean streak spacing and the streamwise distribution of nucleation events.

The spanwise scale of streaky structures has been computed at each streamwise position by means of the auto-correlation function of the streamwise velocity component. Once scaled with the local displacement and momentum thickness, the streak spacing has been shown to converge to 3 and 5, respectively, for all cases. Interestingly, the auto-correlation function of the streamwise velocity component has shown that the streak spacing in the transition region scales well with the displacement and the momentum thickness of the turbulent boundary layer, irrespective of the Reynolds number, Tu level and streamwise pressure gradient.

The computation of the streamwise PDF of spot nucleations allowed discussing the effects of the parameters here tested on the spatial positions where turbulent spots are formed. In this sense, the FST intensity has been found to be the most influencing parameter. At the highest Tu level, the region of highest spot nucleations moves upstream and the PDF width has been shown to significantly increase. This has been ascribed to the elevated number of breakup events occurring as a consequence of streak interactions, which occur randomly in space and time at such elevated free-stream turbulence. On the other hand, when the Reynolds number and the adverse pressure gradient increase, nucleation events are confined in a narrower spatial window and the PDFs are right-skewed.

With the aim of providing a common distribution for the streamwise variation of nucleation events, all the corresponding PDFs have been plotted as function of a newly defined variable accounting for the local values of the streak spacing and the shape factor as well as for the Tu level variation. Interestingly, the nucleation PDFs have been shown to collapse once plotted versus the non-dimensional abscissa here proposed with an acceptable level of approximation. The results discussed in this work suggest that a general shape for the PDF of spot nucleations may be provided accounting for the effects of all the main influencing parameters.

Statistical characterization of free-stream turbulence induced transition

18

DECLARATION OF INTERESTS

The authors report no conflict of interest.

AVAILABILITY OF DATA

The data that support the findings of this study are available from the corresponding author upon reasonable request.

REFERENCES

- ¹K. J. A. Westin, A. V. Boiko, B. G. B. Klingmann, V. V. Kozlov, P. H. Alfredsson, Experiments in a boundary layer subjected to free stream turbulence. part 1. boundary layer structure and receptivity, *J. Fluid Mech.* 281 (1994) 193–218.
- ²J. Kendall, Experiments on boundary-layer receptivity to freestream turbulence, in: 36th AIAA Aerospace Sciences Meeting and Exhibit, 1998, p. 530.
- ³M. Matsubara, P. H. Alfredsson, Disturbance growth in boundary layers subjected to free-stream turbulence, *J. Fluid Mech.* 430 (2001) 149–168.
- ⁴H. W. Emmons, The laminar-turbulent transition in a boundary layer-part i, *Journal of the Aeronautical Sciences* (1951).
- ⁵L. Brandt, F. Schlatter, D. S. Henningson, Transition in boundary layers subject to free-stream turbulence, *J. Fluid Mech.* 517 (2004) 167–198.
- ⁶J. H. Fransson, M. Matsubara, P. H. Alfredsson, Transition induced by free-stream turbulence, *J. Fluid Mech.* 527 (2005) 1–25.
- ⁷K. Nolan, T. Zaki, Conditional sampling of transitional boundary layers in pressure gradients, *J. Fluid Mech.* 728 (2013) 306–339.
- ⁸J. H. Fransson, S. Shahinfar, On the effect of free-stream turbulence on boundary-layer transition, *Journal of Fluid Mechanics* 899 (2020).
- ⁹J. Hunt, P. Durbin, Perturbed vortical layers and shear sheltering, *Fluid dynamics research* 24 (1999) 375.
- ¹⁰R. G. Jacob, P. A. Durbin, Simulations of bypass transition, *J. Fluid Mech.* 428 (2001) 185–212.
- ¹¹T. A. Zaki, S. Saha, On shear sheltering and the structure of vortical modes in single-and two-fluid boundary layers, *Journal of Fluid Mechanics* 626 (2009) 111–147.
- ¹²B. Wang, X. Mao, T. A. Zaki, Low-frequency selectivity in flat-plate boundary layer with elliptic leading edge, *Journal of Fluid Mechanics* 866 (2019) 239–262.
- ¹³P. Sundaram, V. K. Suman, A. Sengupta, T. K. Sengupta, Effects of free stream excitation on the boundary layer over a semi-infinite flat plate, *Physics of Fluids* 32 (2020) 094110.
- ¹⁴J. D. Swearingen, R. F. Blackwelder, The growth and breakdown of streamwise vortices in the presence of a wall, *Journal of Fluid Mechanics* 182 (1987) 255–290.
- ¹⁵P. Andersson, L. Brandt, A. Bottaro, D. S. Henningson, On the breakdown of boundary layers streaks, *J. Fluid Mech.* 428 (2001) 29–60.
- ¹⁶L. Brandt, D. S. Henningson, Transition of streamwise streaks in zero-pressure-gradient boundary layers, *Journal of Fluid Mechanics* 472 (2002) 229–261.
- ¹⁷M. Asai, M. Minagawa, M. Nishioka, The instability and breakdown of a near-wall low-speed streak, *Journal of Fluid Mechanics* 455 (2002) 289–314.
- ¹⁸J. Mans, H. De Lange, A. Van Steenhoven, Sinuous breakdown in a flat plate boundary layer exposed to free-stream turbulence, *Physics of Fluids* 19 (2007) 088101.
- ¹⁹P. Schlatter, L. Brandt, H. De Lange, D. S. Henningson, On streak breakdown in bypass transition, *Physics of fluids* 20 (2008) 101505.
- ²⁰J. Mans, E. C. Kadijk, H. C. de Lange, A. A. van Steenhoven, Breakdown in a boundary layer exposed to free-stream turbulence, *Exp Fluids* 39 (2005) 1071–1083.
- ²¹A. Zhang, M. Dong, Y. Zhang, Receptivity of secondary instability modes in streaky boundary layers, *Physics of Fluids* 30 (2018) 114102.
- ²²L. Brandt, H. C. De Lange, Streaks interaction and breakdown in boundary layer flows, *Phys. Fluids* 20 (2008) 024107–1–024107–16.
- ²³O. Marxen, T. A. Zaki, Turbulence in intermittent transitional boundary layers and in turbulence spots, *Journal of Fluid Mechanics* 860 (2019) 350–383.
- ²⁴D. Goldstein, J. Chu, G. Brown, Lateral spreading mechanism of a turbulent spot and a turbulent wedge, *Flow, Turbulence and Combustion* 98 (2017) 21–35.
- ²⁵C. Lee, X. Jiang, Flow structures in transitional and turbulent boundary layers, *Physics of Fluids* 31 (2019) 111301.
- ²⁶L. Klotz, J. E. Wesfreid, Experiments on transient growth of turbulent spots, *Journal of Fluid Mechanics* 829 (2017).
- ²⁷D. Hermon, E. J. Walsh, D. M. McELIGOT, Experimental investigation into the routes to bypass transition and the shear-sheltering phenomenon, *Journal of Fluid Mechanics* 591 (2007) 461.
- ²⁸R. G. Jacobs, P. A. Durbin, Shear sheltering and the continuous spectrum of the Orr-Sommerfeld equation, *Physics of Fluids* 10 (1998) 2006–2011.
- ²⁹K. P. Nolan, E. J. Walsh, Particle image velocimetry measurements of a transitional boundary layer under free stream turbulence, *J. Fluid Mech.* 702 (2012) 215–238.
- ³⁰X. Ruan, X. Zhang, P. Wang, W. Liu, L. Hu, Z. Xu, Investigation on the boundary layer transition with the effects of periodic passing wakes, *Physics of Fluids* 32 (2020) 125113.
- ³¹H. Albiez, C. Gramesbacher, M. Stripf, H.-J. Bauer, High-resolution measurements of heat transfer, near-wall intermittency, and reynolds-stresses along a flat plate boundary layer undergoing bypass transition, *Journal of Heat Transfer* 142 (2020).
- ³²D. Veerasamy, C. J. Atkin, S. A. Ponnusami, Aerofoil wake-induced transition characteristics on a flat-plate boundary layer, *Journal of Fluid Mechanics* 920 (2021).
- ³³T. A. Zaki, P. A. Durbin, Continuous mode transition and the effects of pressure gradient, *J. Fluid Mech.* 563 (2006) 357–388.
- ³⁴T. Zaki, From streaks to spots and on to turbulence: Exploring the dynamics of boundary layer transition, *Flow Turbul. and Combust.* 91 (2013) 451–473.
- ³⁵X. Wang, Z. Wang, M. Sun, Q. Wang, Z. Hu, Effects of favorable pressure gradient on turbulence structures and statistics of a flat-plate supersonic turbulent boundary layer, *Physics of Fluids* 32 (2020) 025107.
- ³⁶S. Suryanarayanan, D. B. Goldstein, A. R. Berger, E. B. White, G. L. Brown, Effect of pressure gradients on the different stages of roughness induced boundary layer transition, *International Journal of Heat and Fluid Flow* 86 (2020) 108688.
- ³⁷D. Veerasamy, C. Atkin, A rational method for determining intermittency in the transitional boundary layer, *Experiments in Fluids* 61 (2020) 1–13.
- ³⁸N. Otsu, A threshold selection method from gray-level histograms, *IEEE transactions on systems, man, and cybernetics* 9 (1979) 62–66.
- ³⁹T. Kreilos, T. Khapko, P. Schlatter, Y. Duguet, D. S. Henningson, B. Eckhardt, Bypass transition and spot nucleation in boundary layers, *Physical Review Fluids* 1 (2016) 043602.
- ⁴⁰J. Lee, T. Zaki, Signature of large-scale motions on turbulent/non-turbulent interface in boundary layers, *Journal of Fluid Mechanics* 819 (2017) 165–187.
- ⁴¹T. K. Sengupta, P. K. Sharma, A. Sengupta, V. K. Suman, Tracking disturbances in transitional and turbulent flows: Coherent structures, *Physics of Fluids* 31 (2019) 124106.
- ⁴²D. Simoni, D. Lengani, M. Dellacasagrande, S. Kubacki, E. Dick, An accurate data base on laminar-to-turbulent transition in variable pressure gradient flows, *International Journal of Heat and Fluid Flow* 77 (2019) 84–97.
- ⁴³M. Dellacasagrande, J. Verdoya, D. Barsi, D. Lengani, D. Simoni, Mixed lse and epod based technique for multi-plane piv measurements synchronization in separated flow condition, *Experimental Thermal and Fluid Science* 122 (2021) 110313.
- ⁴⁴A. Sciacchitano, D. R. Neal, B. L. Smith, S. O. Warner, P. P. Vlachos, B. Wieneke, F. Scarano, Collaborative framework for piv uncertainty quantification: comparative assessment of methods, *Measurement Science and Technology* 26 (2015) 074004.
- ⁴⁵B. Wieneke, PIV uncertainty quantification from correlation statistics, *Measurement Science and Technology* 26 (2015) 074002.

This is the author's peer reviewed, accepted manuscript. However, the online version of record will be different from this version once it has been copyedited and typeset.

PLEASE CITE THIS ARTICLE AS DOI: 10.1063/1.50063948

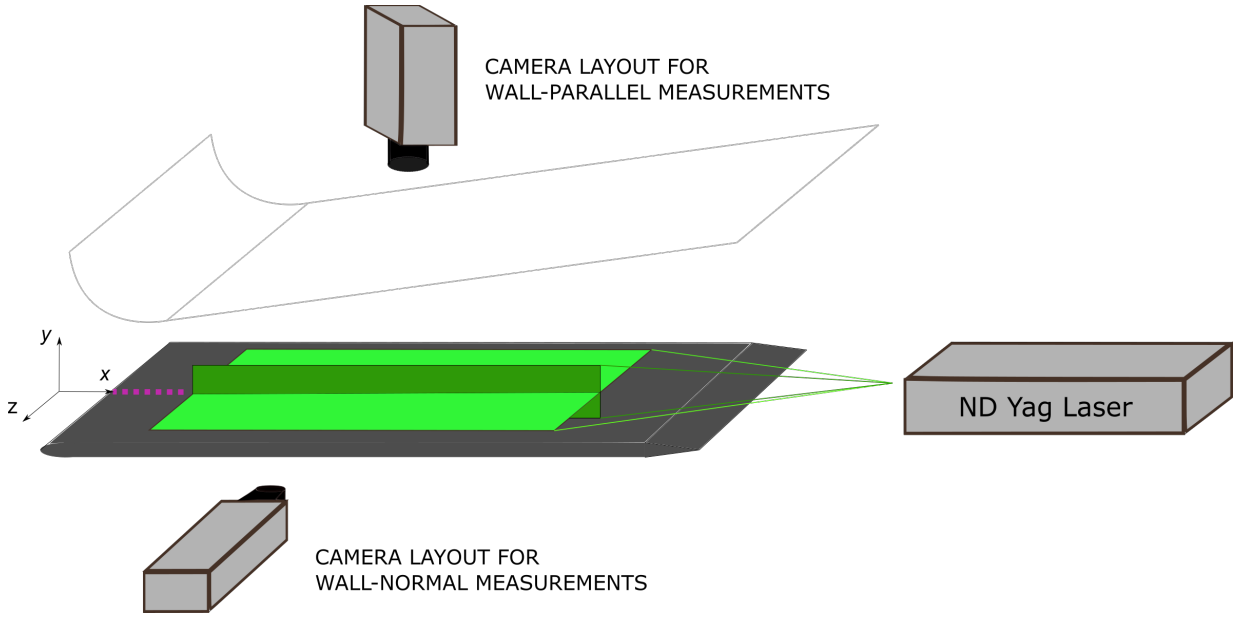
Statistical characterization of free-stream turbulence induced transition

19

- ⁴⁶M. Dellacasagrande, D. Barsi, D. Lengani, D. Simoni, J. Verdoya, Response of a flat plate laminar separation bubble to Reynolds number, free-stream turbulence and adverse pressure gradient variation, *Experiments in Fluids* 61 (2020).
- ⁴⁷J. Verdoya, M. Dellacasagrande, D. Lengani, D. Simoni, M. Ubaldi, Inspection of structures interaction in laminar separation bubbles with extended proper orthogonal decomposition applied to multi-plane particle image velocimetry data, *Physics of Fluids* 33 (2021) 043607.
- ⁴⁸R. Narasimha, K. Devasia, G. Gururani, M. B. Narayanan, Transitional intermittency in boundary layers subjected to pressure gradient, *Experiments in Fluids* 2 (1984) 171–176.
- ⁴⁹J. L. Lumley, Stochastic tools in turbulence, *Applied Mathematics and Mechanics*, vol. 12 (1970).
- ⁵⁰K. Nolan, E. Walsh, D. McEligot, Quadrant analysis of a transitional boundary layer subject to free-stream turbulence, *Journal of fluid mechanics* 658 (2010) 310.
- ⁵¹R. J. Adrian, Hairpin vortex organization in wall turbulence, *Phys. Fluids* 19 (2007) 041301–1–041301–16.
- ⁵²L. Brandt, C. Cossu, J.-M. Chomaz, P. Huerre, D. S. Henningson, On the convectively unstable nature of optimal streaks in boundary layers, *Journal of Fluid Mechanics* 485 (2003) 221–242.
- ⁵³B. Abu-Ghannam, R. Shaw, Natural transition of boundary layers—the effects of turbulence, pressure gradient, and flow history, *Journal of Mechanical Engineering Science* 22 (1980) 213–228.

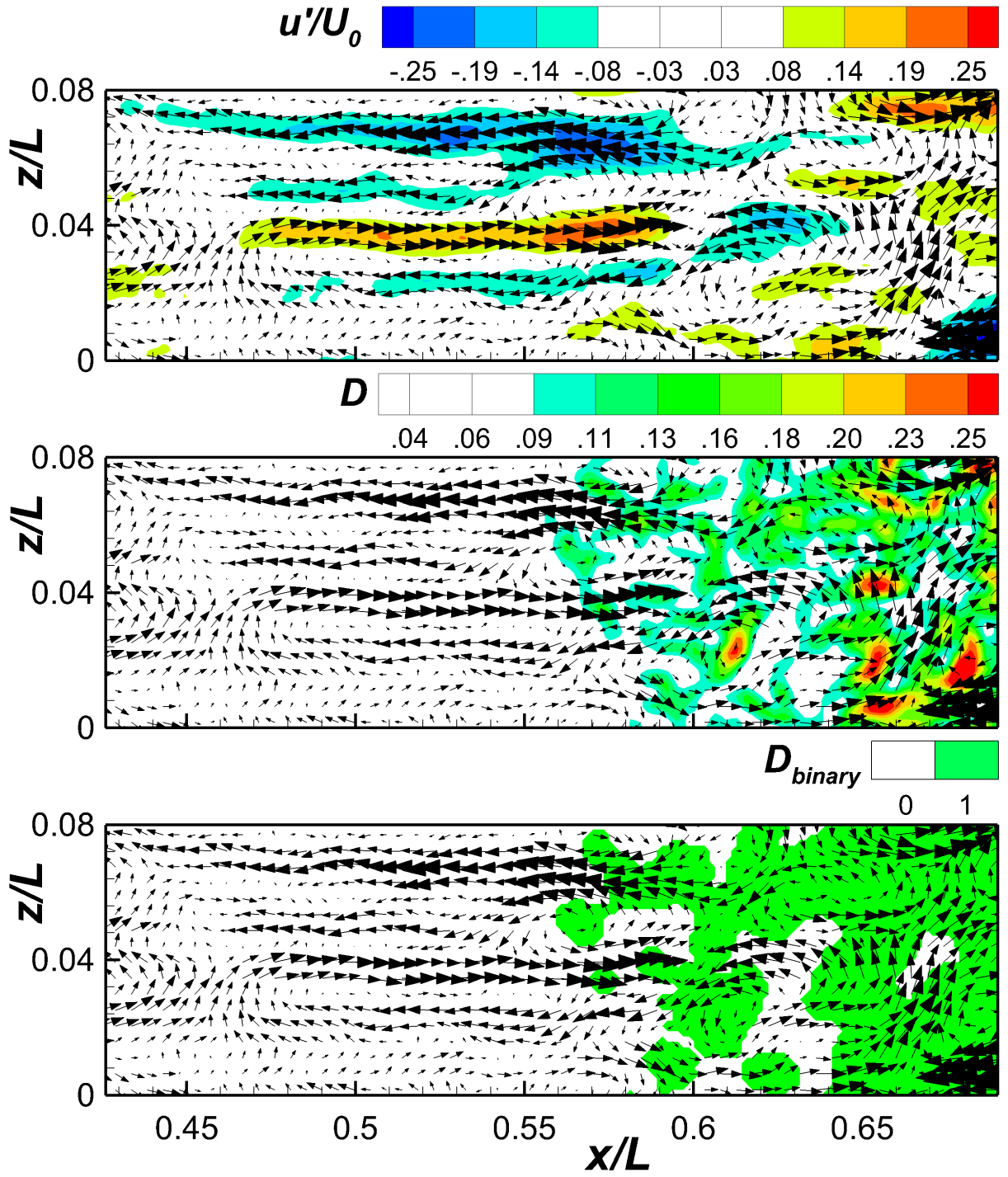
This is the author's peer reviewed, accepted manuscript. However, the online version of record will be different from this version once it has been copyedited and typeset.

PLEASE CITE THIS ARTICLE AS DOI: 10.1063/1.50063948



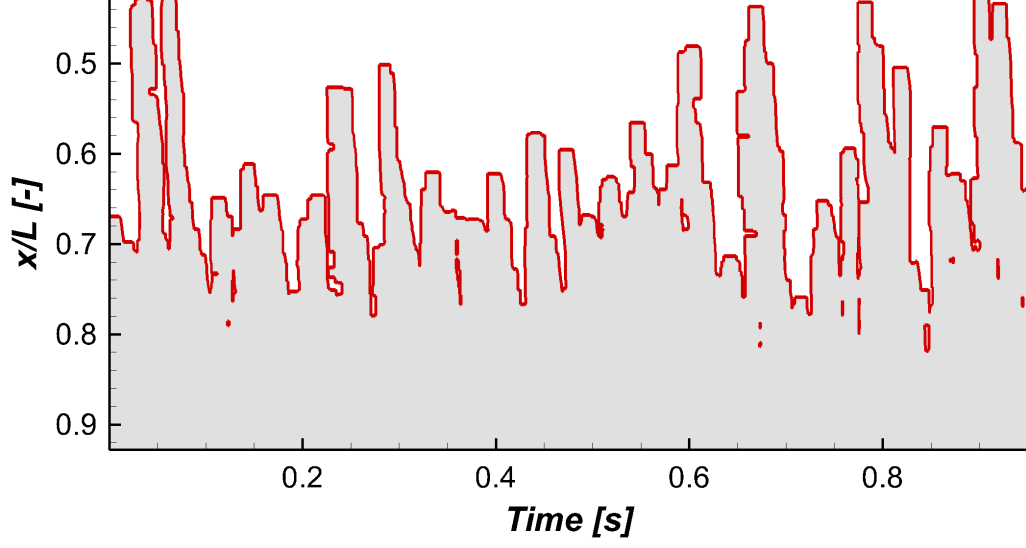
This is the author's peer reviewed, accepted manuscript. However, the online version of record will be different from this version once it has been copyedited and typeset.

PLEASE CITE THIS ARTICLE AS DOI: 10.1063/1.50063948



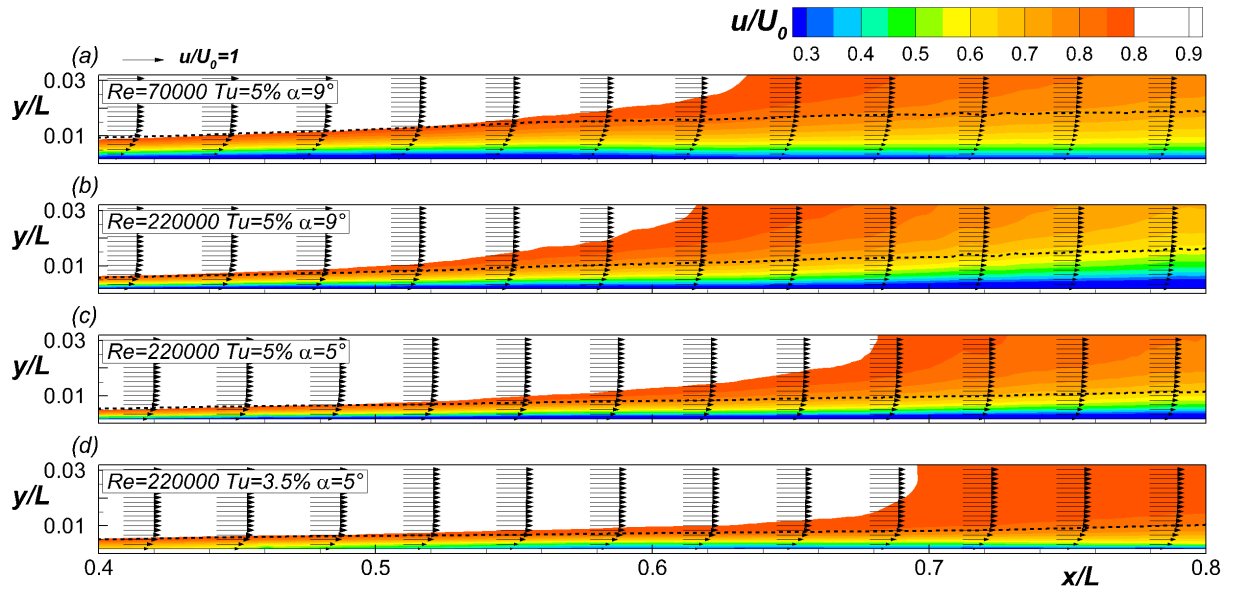
This is the author's peer reviewed, accepted manuscript. However, the online version of record will be different from this version once it has been copyedited and typeset.

PLEASE CITE THIS ARTICLE AS DOI: 10.1063/1.50063948



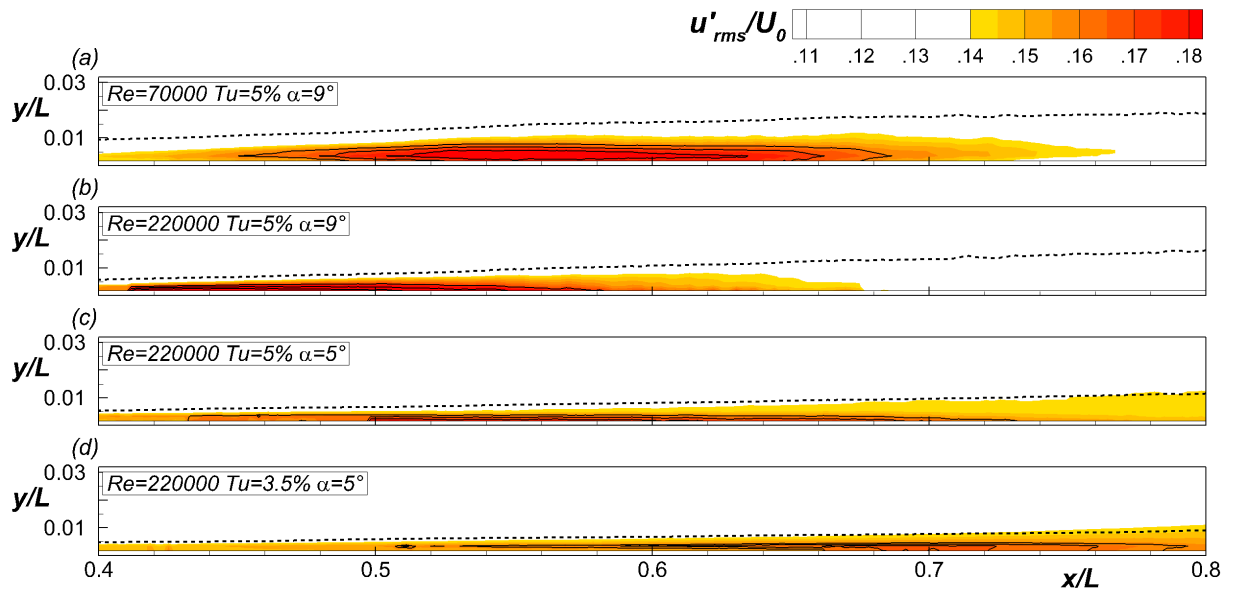
This is the author's peer reviewed, accepted manuscript. However, the online version of record will be different from this version once it has been copyedited and typeset.

PLEASE CITE THIS ARTICLE AS DOI: 10.1063/1.50063948



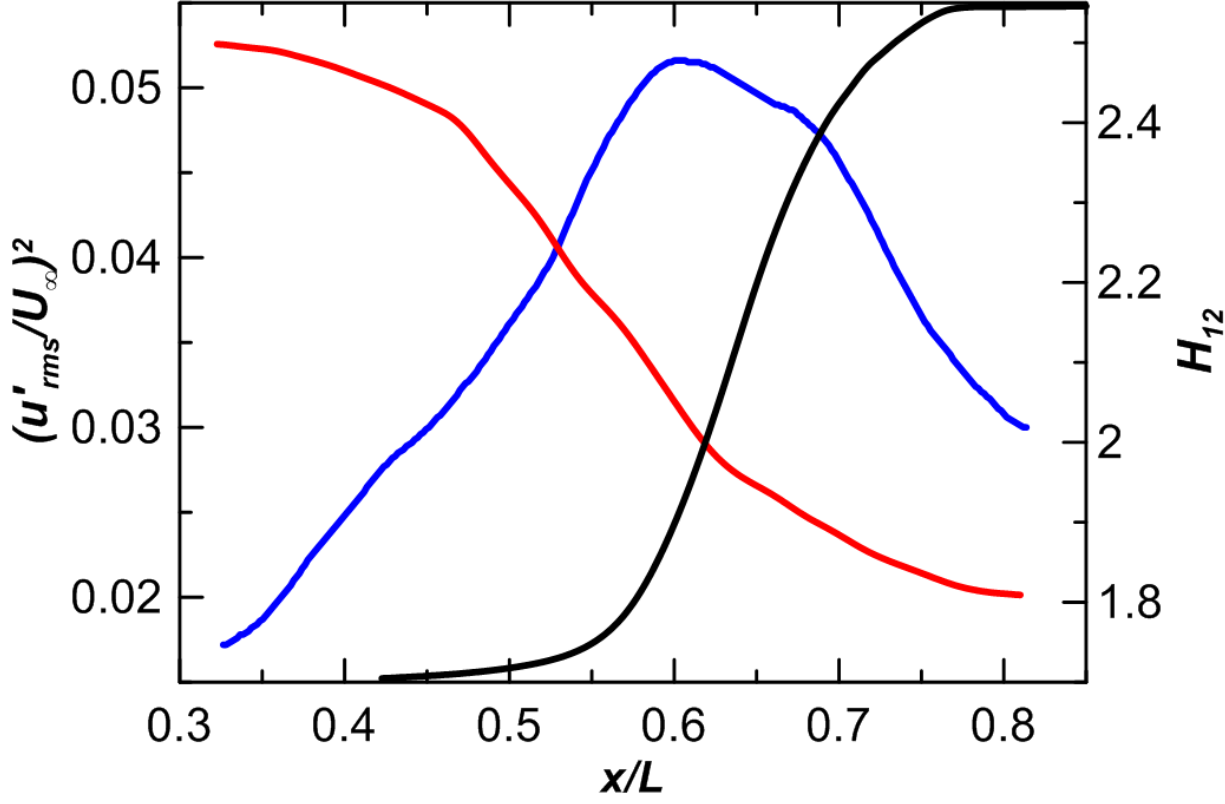
This is the author's peer reviewed, accepted manuscript. However, the online version of record will be different from this version once it has been copyedited and typeset.

PLEASE CITE THIS ARTICLE AS DOI: 10.1063/1.50063948



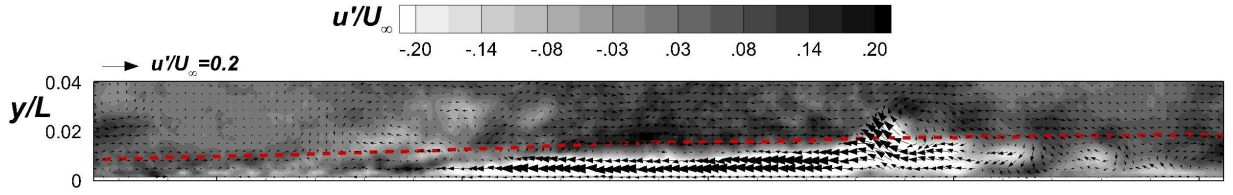
This is the author's peer reviewed, accepted manuscript. However, the online version of record will be different from this version once it has been copyedited and typeset.

PLEASE CITE THIS ARTICLE AS DOI: 10.1063/5.0063948



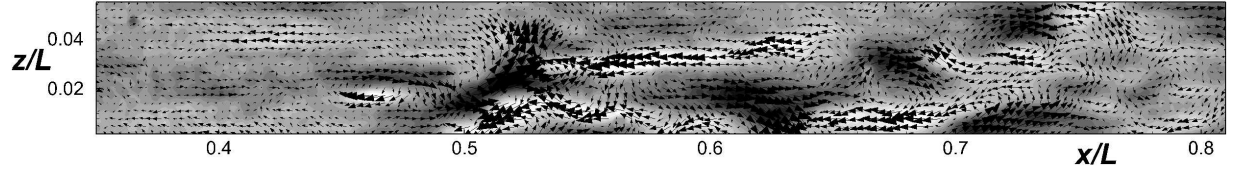
This is the author's peer reviewed, accepted manuscript. However, the online version of record will be different from this version once it has been copyedited and typeset.

PLEASE CITE THIS ARTICLE AS DOI: 10.1063/1.50063948



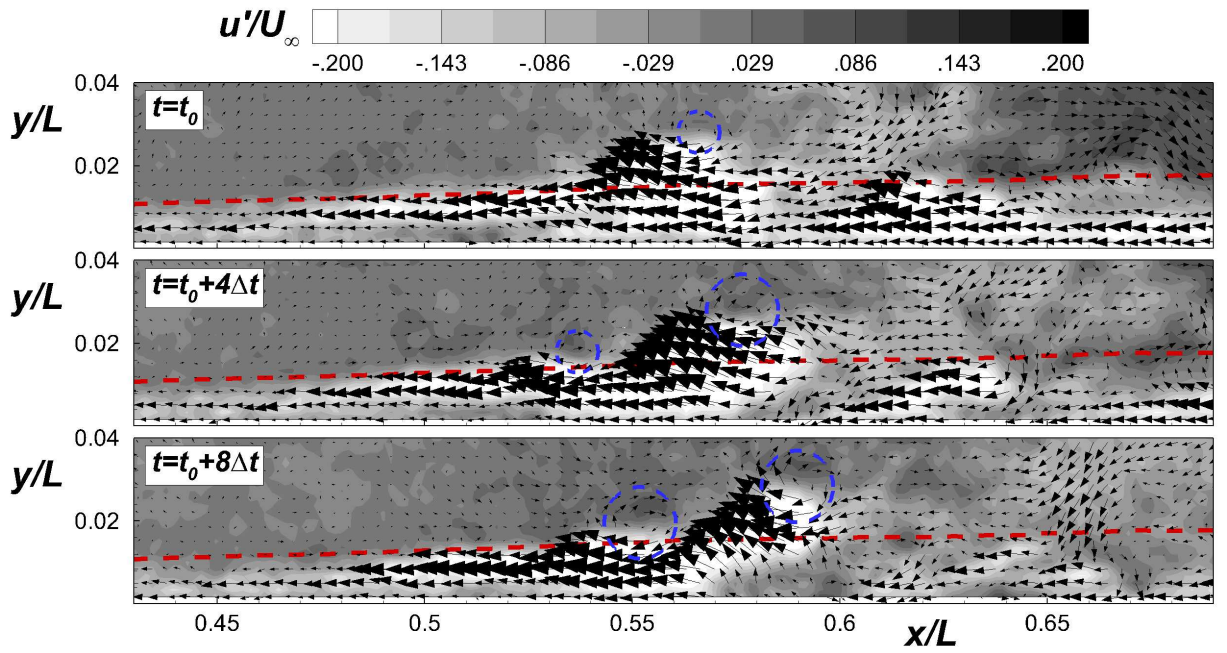
This is the author's peer reviewed, accepted manuscript. However, the online version of record will be different from this version once it has been copyedited and typeset.

PLEASE CITE THIS ARTICLE AS DOI: 10.1063/1.50063948



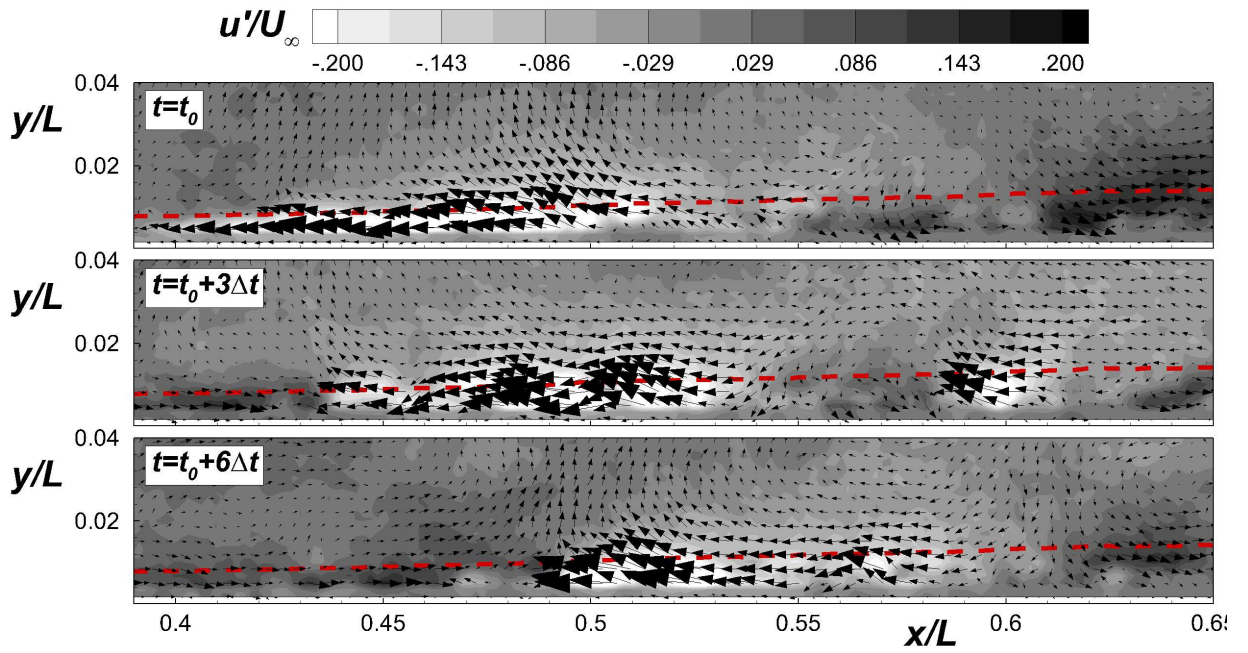
This is the author's peer reviewed, accepted manuscript. However, the online version of record will be different from this version once it has been copyedited and typeset.

PLEASE CITE THIS ARTICLE AS DOI: 10.1063/1.50063948



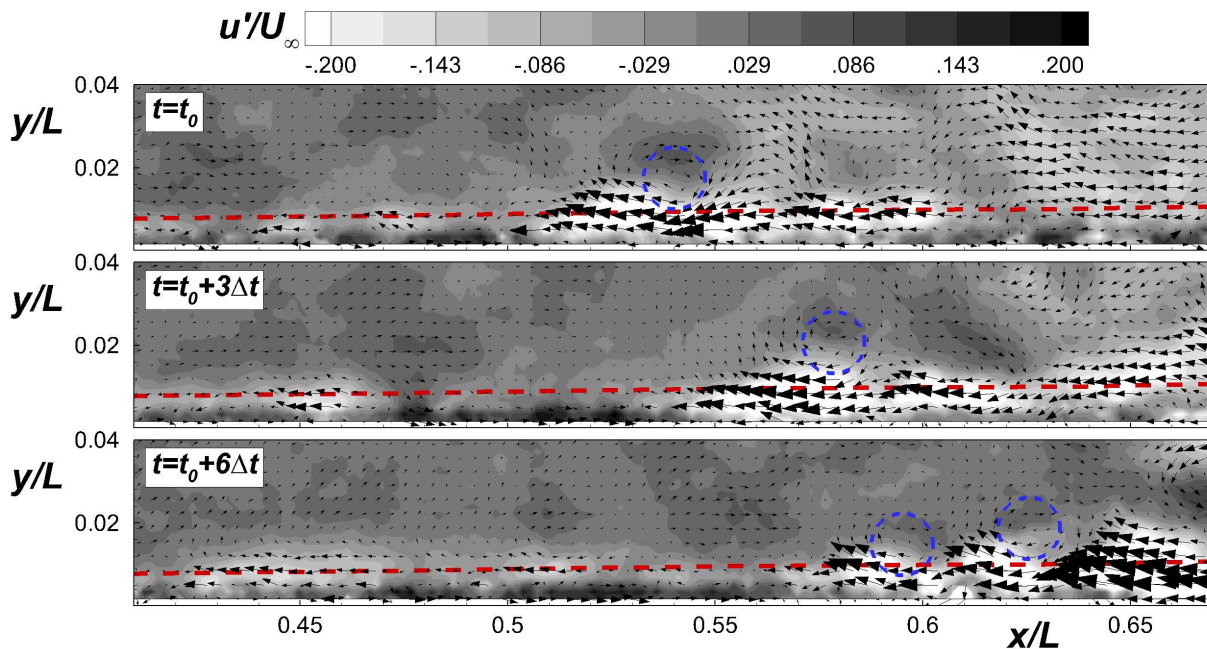
This is the author's peer reviewed, accepted manuscript. However, the online version of record will be different from this version once it has been copyedited and typeset.

PLEASE CITE THIS ARTICLE AS DOI: 10.1063/1.50063948



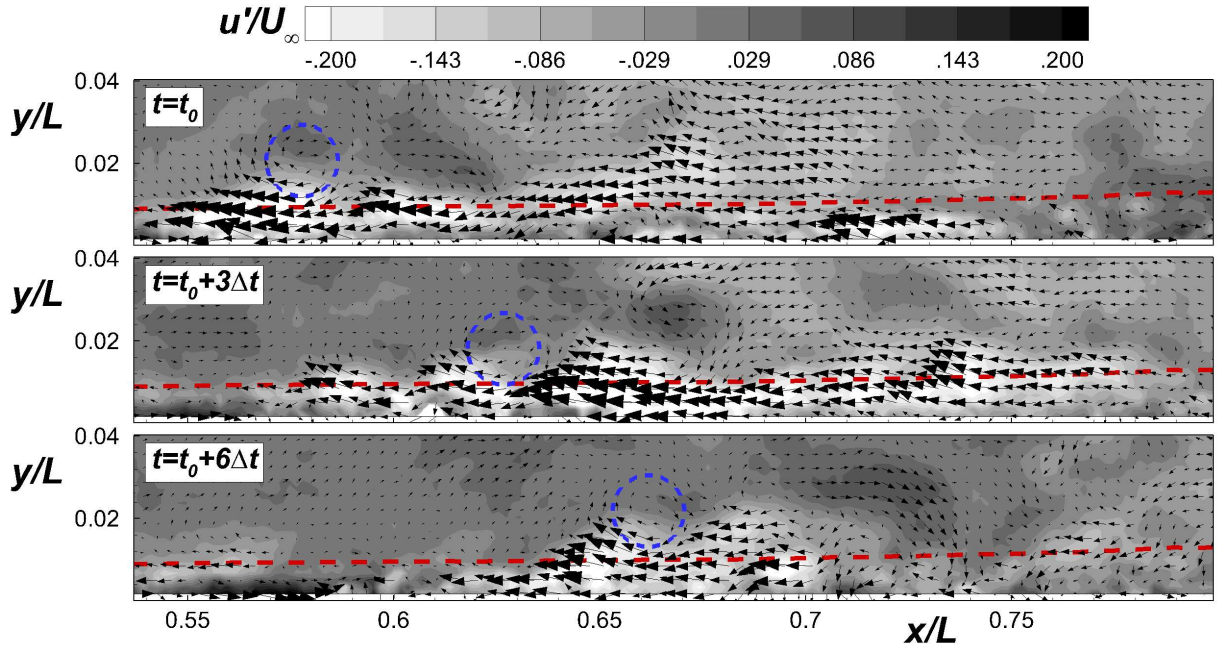
This is the author's peer reviewed, accepted manuscript. However, the online version of record will be different from this version once it has been copyedited and typeset.

PLEASE CITE THIS ARTICLE AS DOI: 10.1063/1.50063948



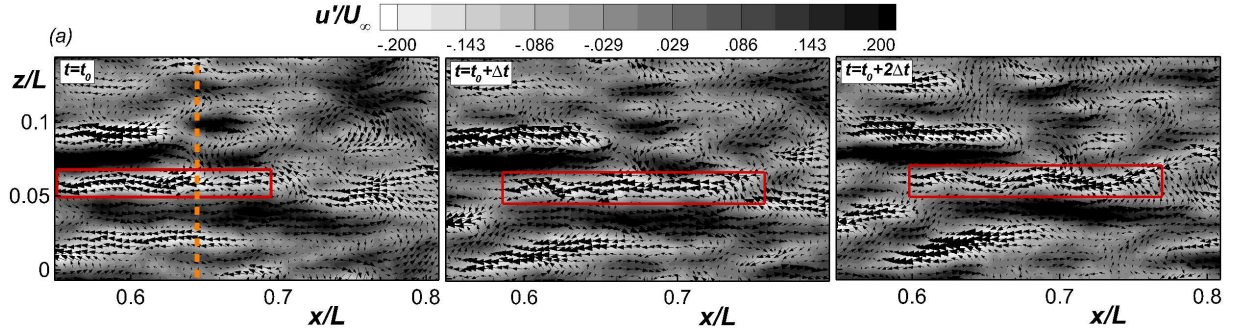
This is the author's peer reviewed, accepted manuscript. However, the online version of record will be different from this version once it has been copyedited and typeset.

PLEASE CITE THIS ARTICLE AS DOI: 10.1063/1.50063948



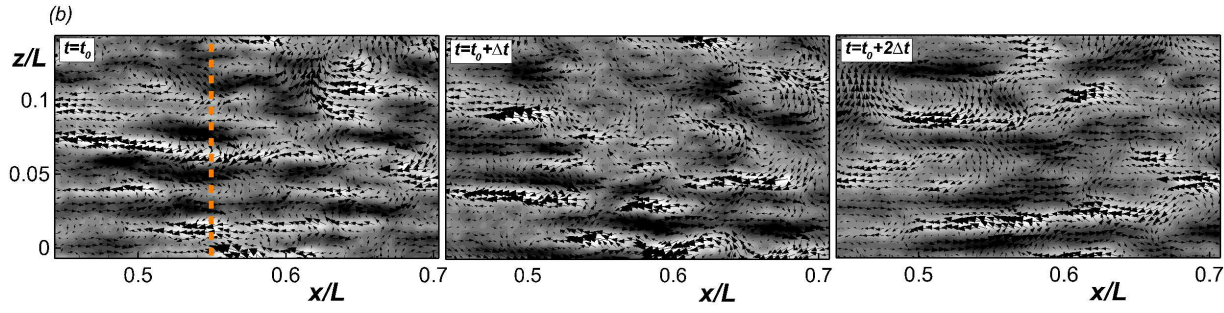
This is the author's peer reviewed, accepted manuscript. However, the online version of record will be different from this version once it has been copyedited and typeset.

PLEASE CITE THIS ARTICLE AS DOI: 10.1063/1.50063948



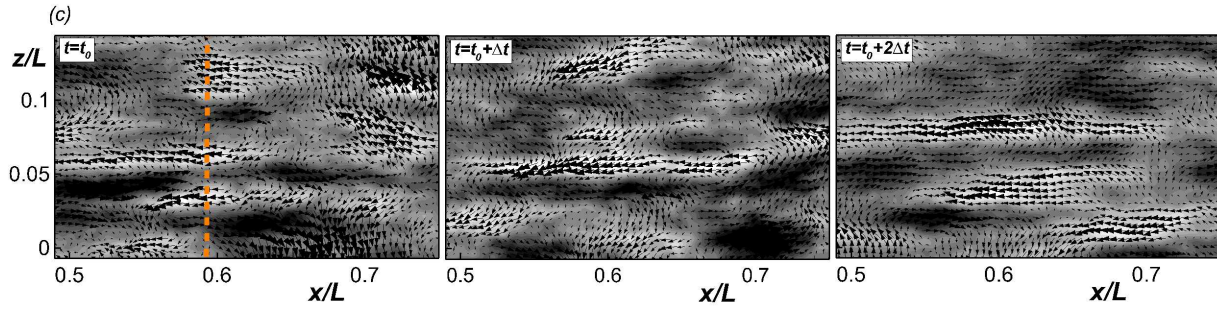
This is the author's peer reviewed, accepted manuscript. However, the online version of record will be different from this version once it has been copyedited and typeset.

PLEASE CITE THIS ARTICLE AS DOI: 10.1063/1.50063948



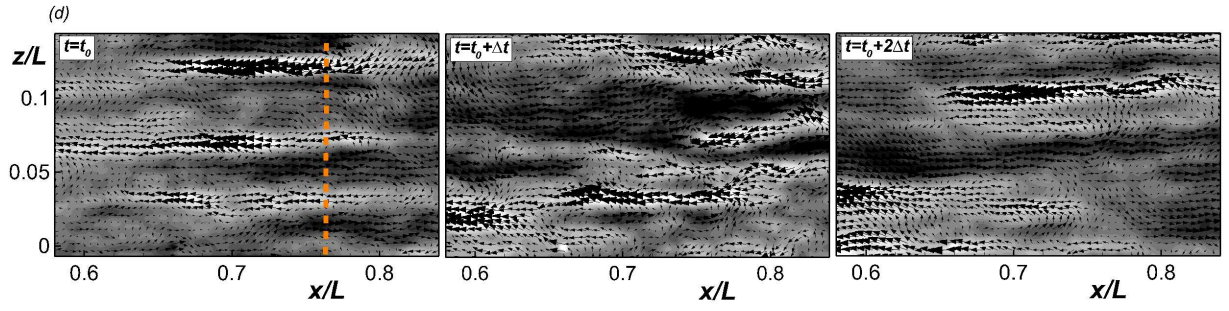
This is the author's peer reviewed, accepted manuscript. However, the online version of record will be different from this version once it has been copyedited and typeset.

PLEASE CITE THIS ARTICLE AS DOI: 10.1063/1.50063948



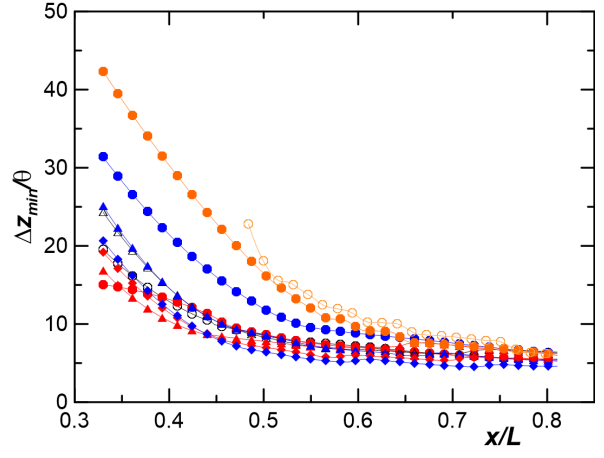
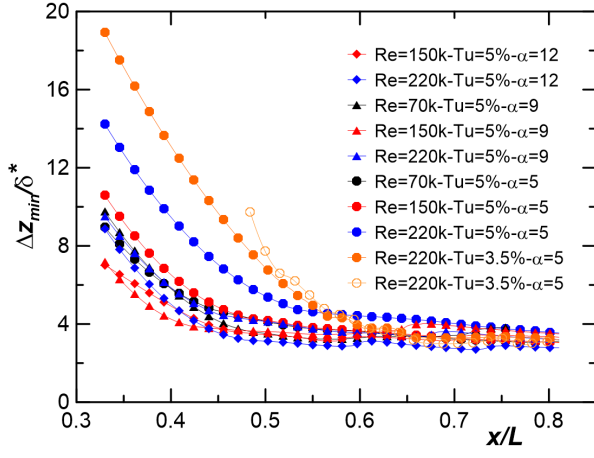
This is the author's peer reviewed, accepted manuscript. However, the online version of record will be different from this version once it has been copyedited and typeset.

PLEASE CITE THIS ARTICLE AS DOI: 10.1063/1.50063948



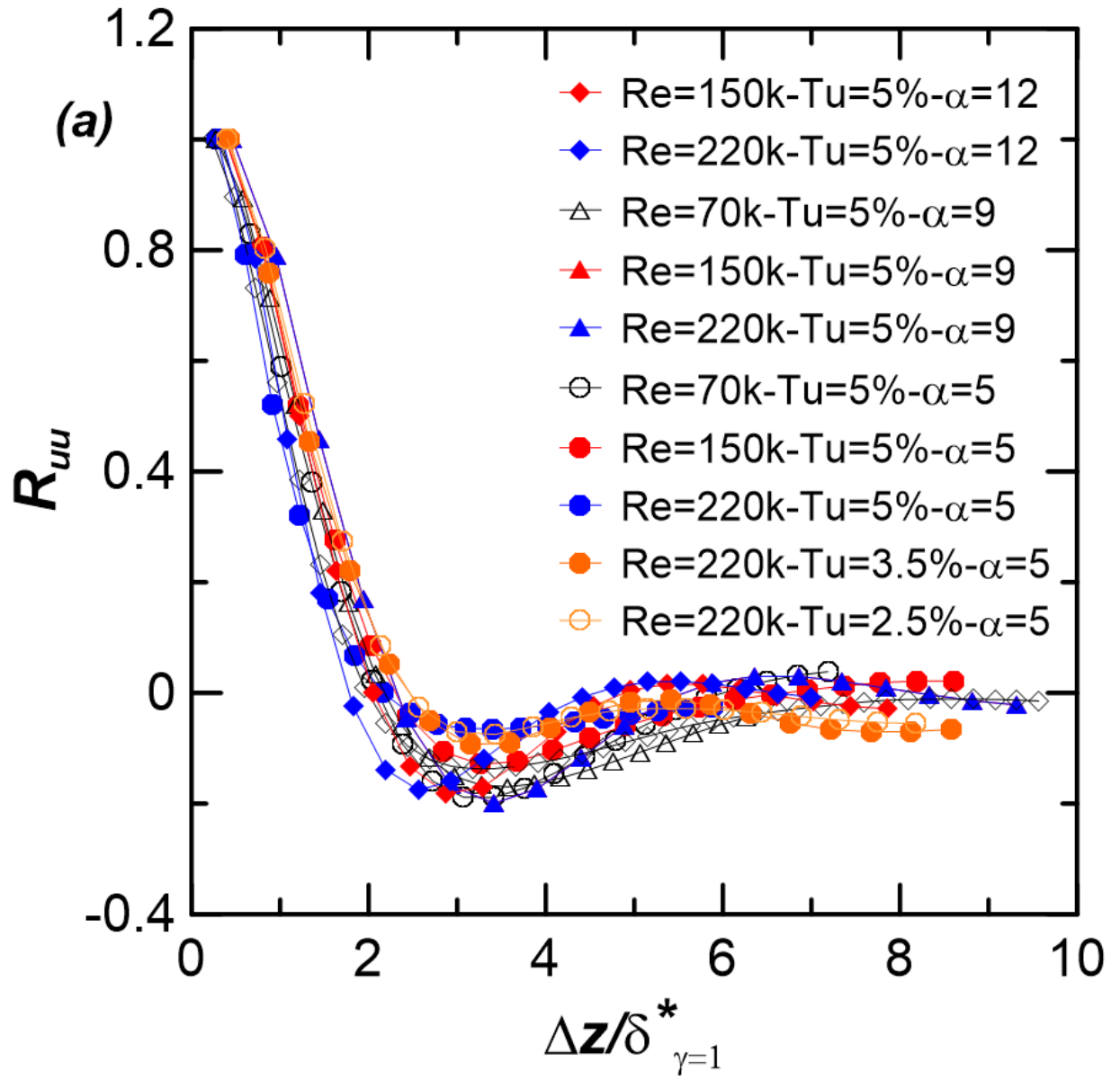
This is the author's peer reviewed, accepted manuscript. However, the online version of record will be different from this version once it has been copyedited and typeset.

PLEASE CITE THIS ARTICLE AS DOI: 10.1063/1.50063948

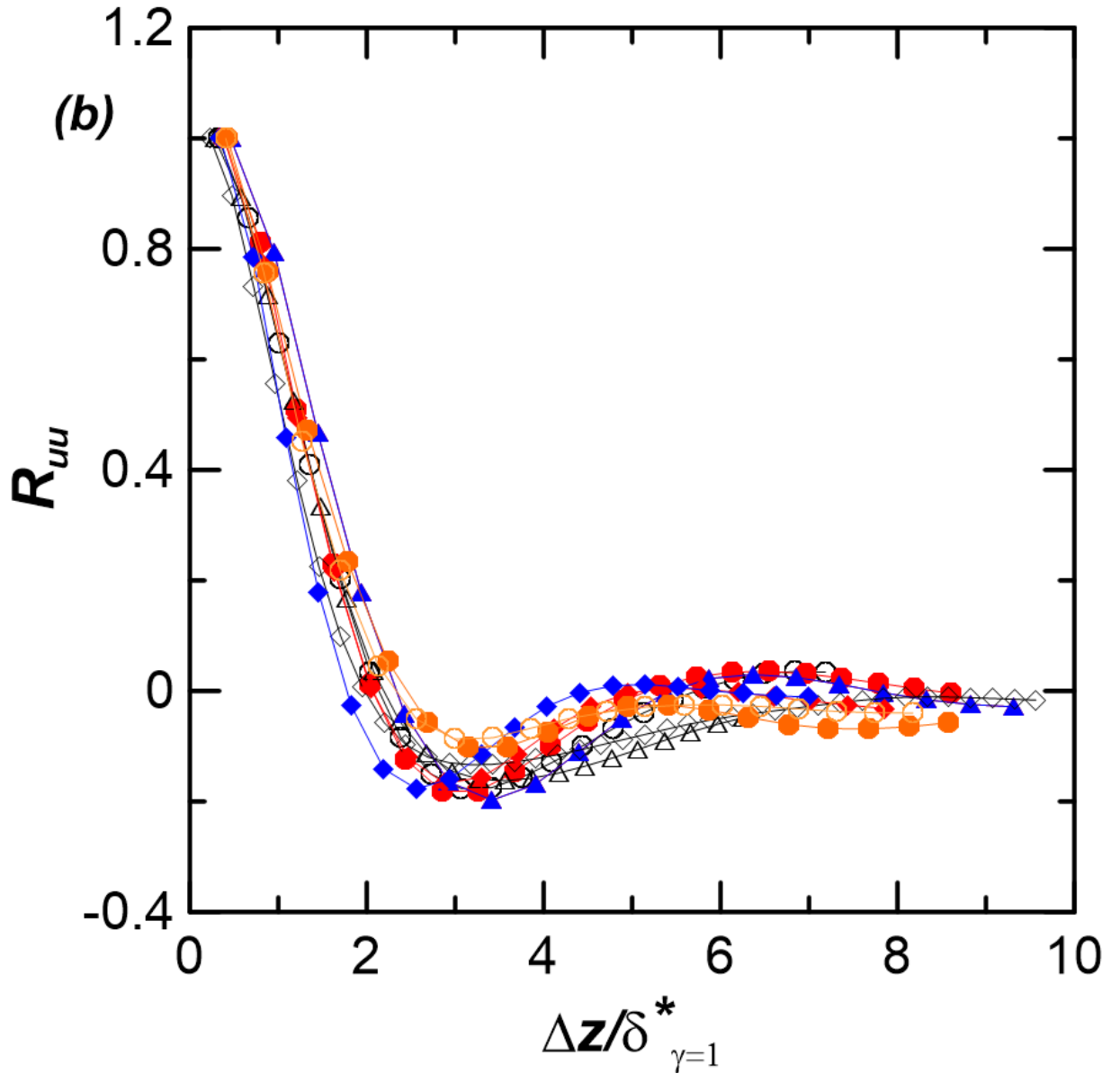


This is the author's peer reviewed, accepted manuscript. However, the online version of record will be different from this version once it has been copyedited and typeset.

PLEASE CITE THIS ARTICLE AS DOI: 10.1063/1.50063948

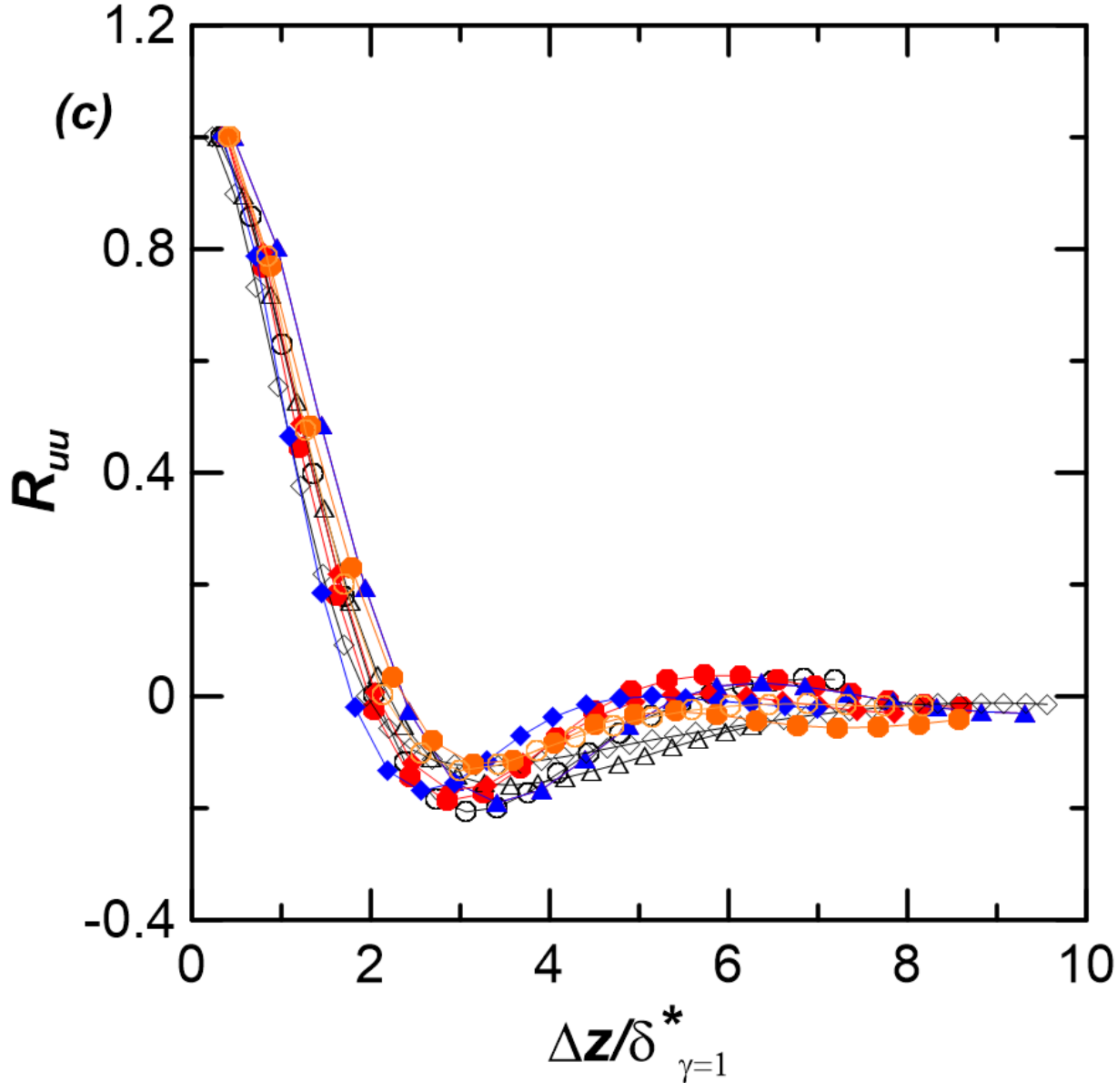


This is the author's peer reviewed, accepted manuscript. However, the online version of record will be different from this version once it has been copyedited and typeset.
 PLEASE CITE THIS ARTICLE AS DOI: 10.1063/1.50063948



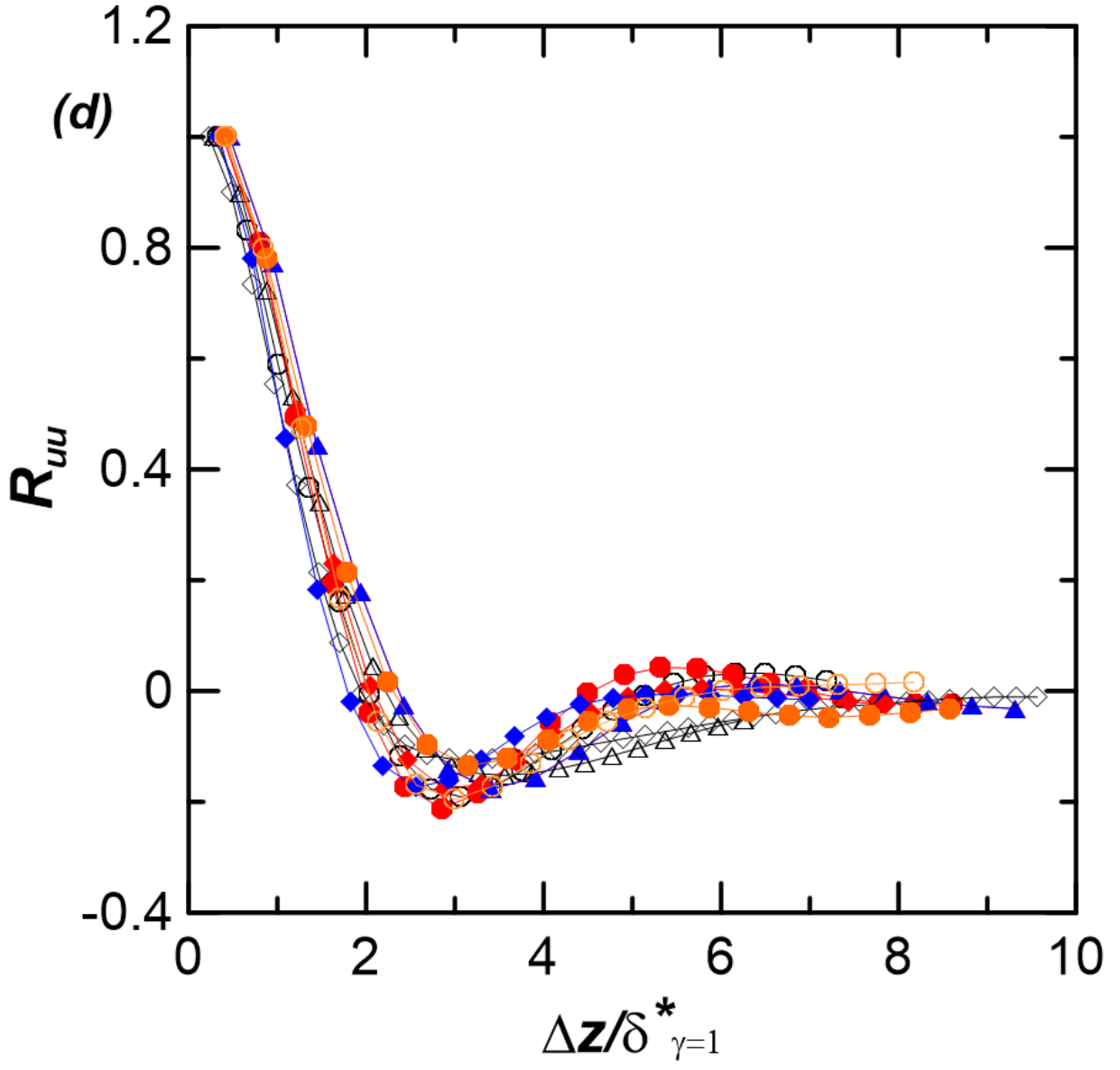
This is the author's peer reviewed, accepted manuscript. However, the online version of record will be different from this version once it has been copyedited and typeset.

PLEASE CITE THIS ARTICLE AS DOI: 10.1063/1.50063948



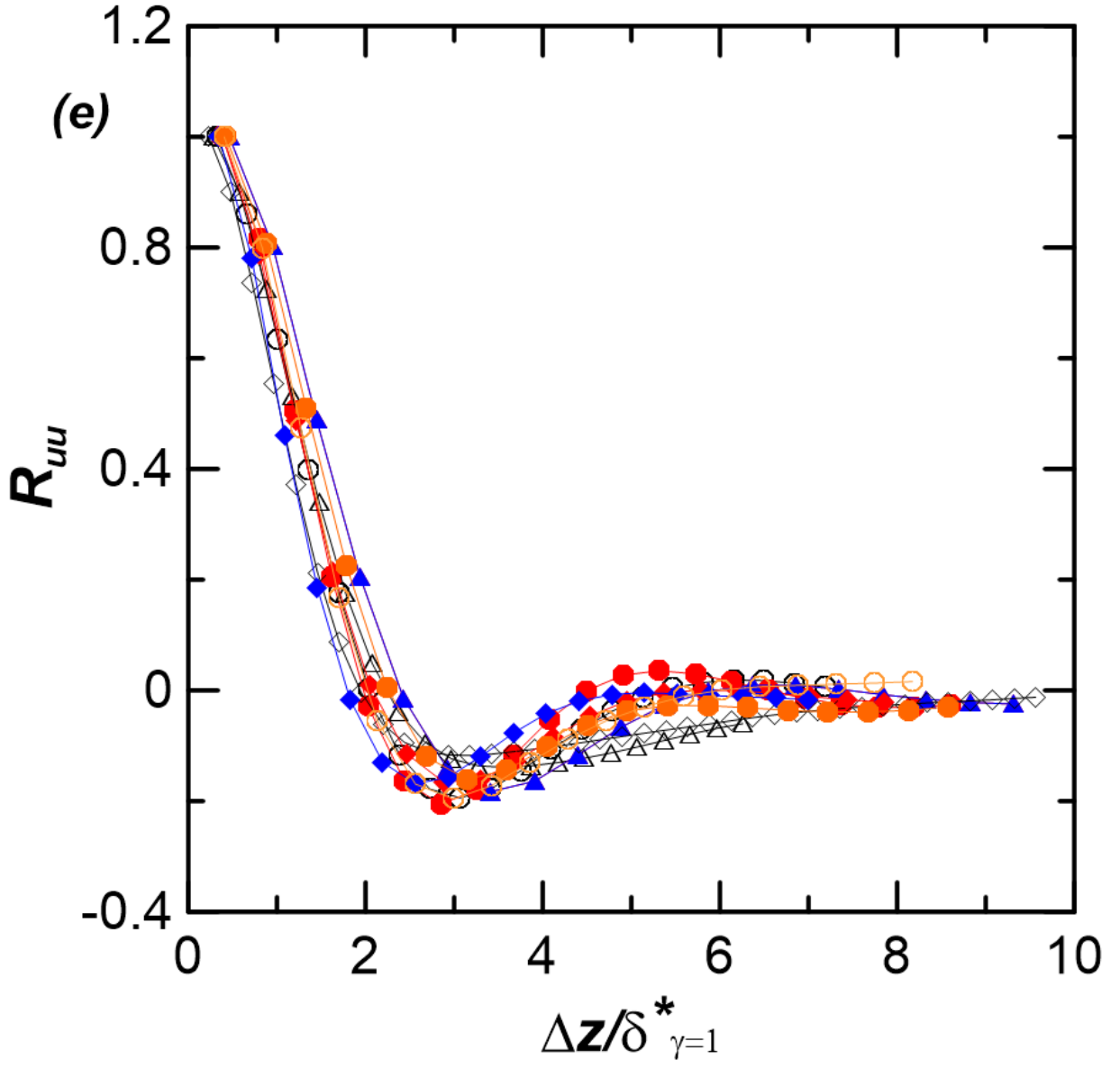
This is the author's peer reviewed, accepted manuscript. However, the online version of record will be different from this version once it has been copyedited and typeset.

PLEASE CITE THIS ARTICLE AS DOI: 10.1063/1.50063948



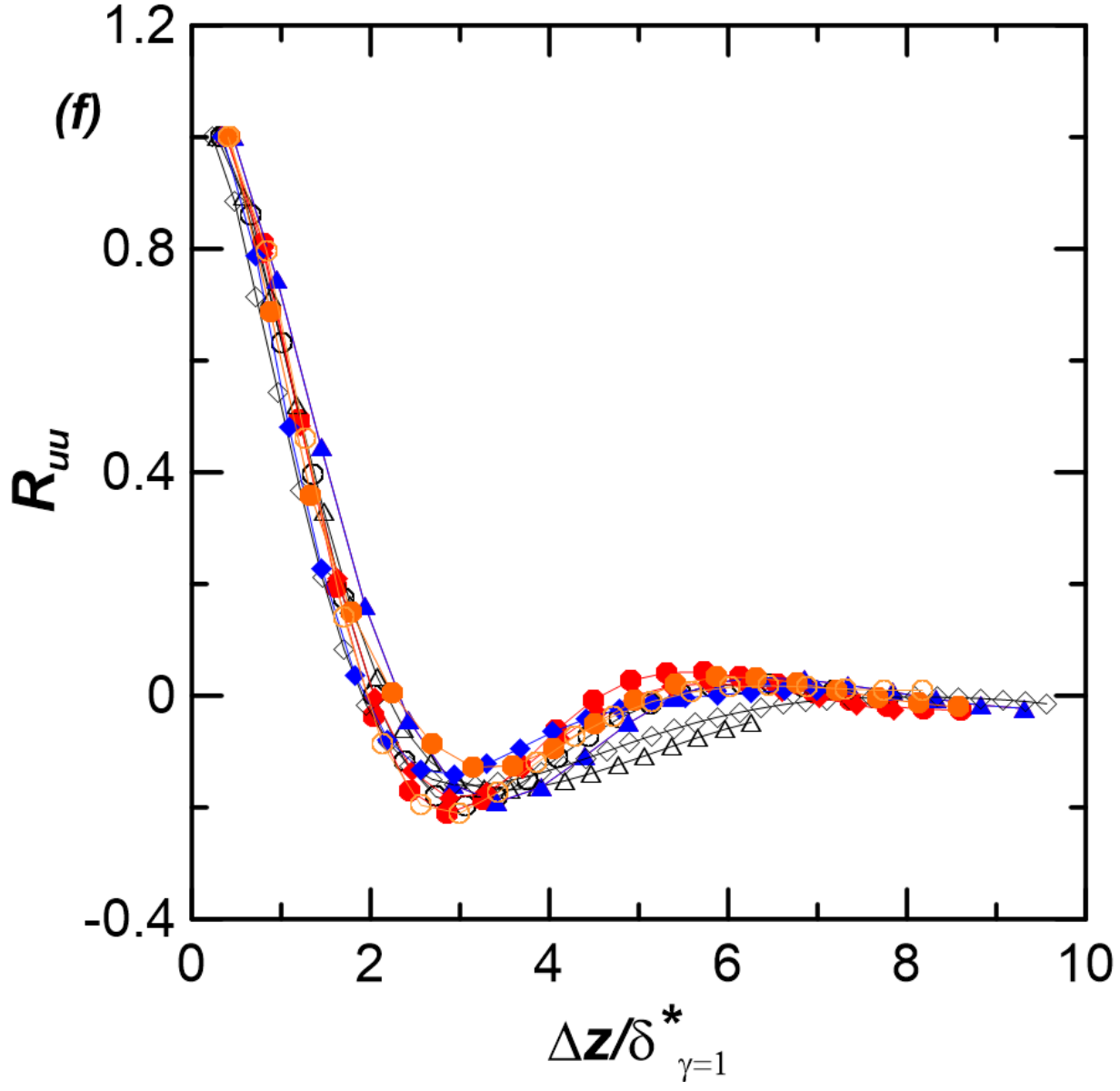
This is the author's peer reviewed, accepted manuscript. However, the online version of record will be different from this version once it has been copyedited and typeset.

PLEASE CITE THIS ARTICLE AS DOI: 10.1063/1.50063948



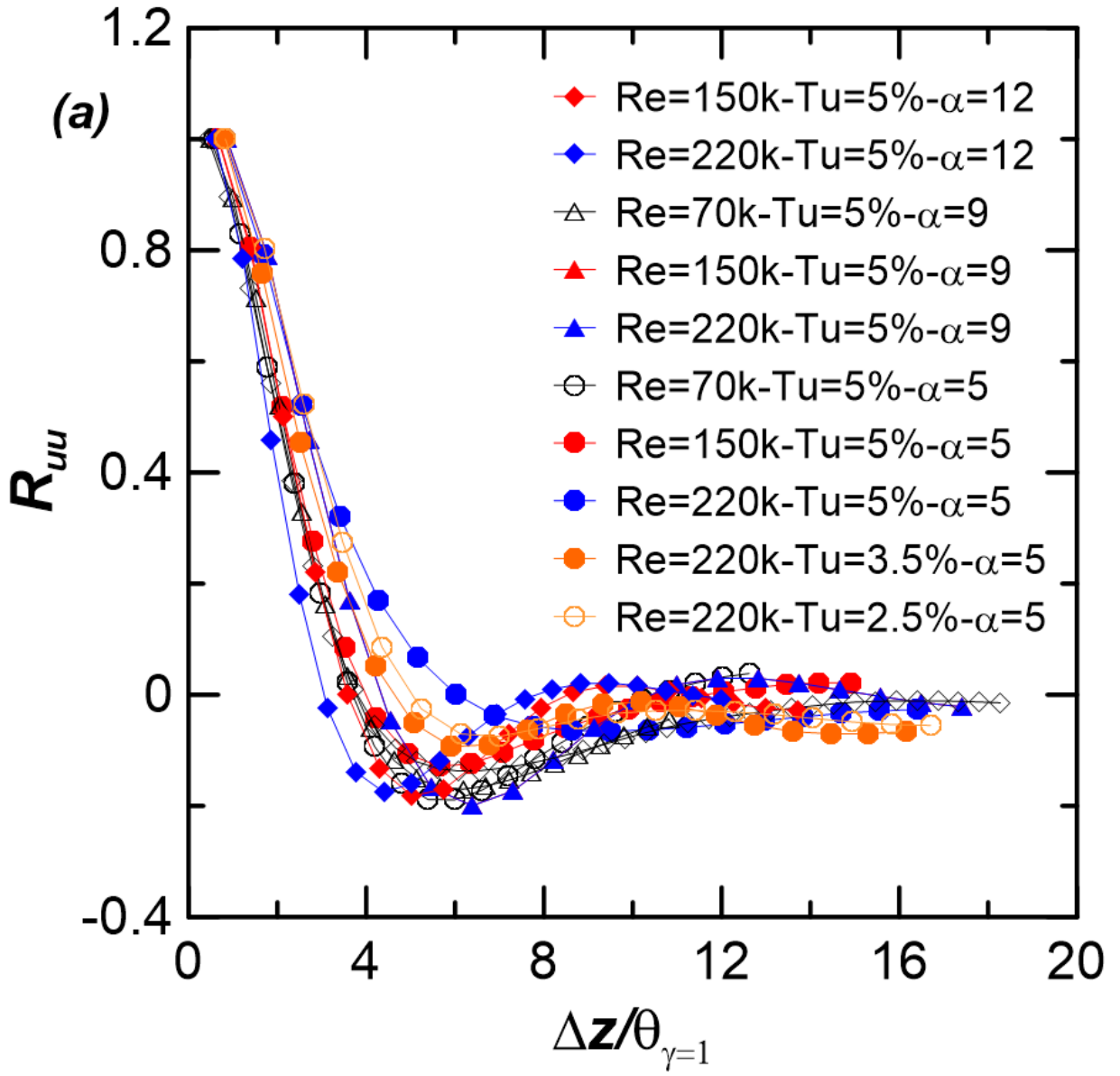
This is the author's peer reviewed, accepted manuscript. However, the online version of record will be different from this version once it has been copyedited and typeset.

PLEASE CITE THIS ARTICLE AS DOI: 10.1063/1.50063948



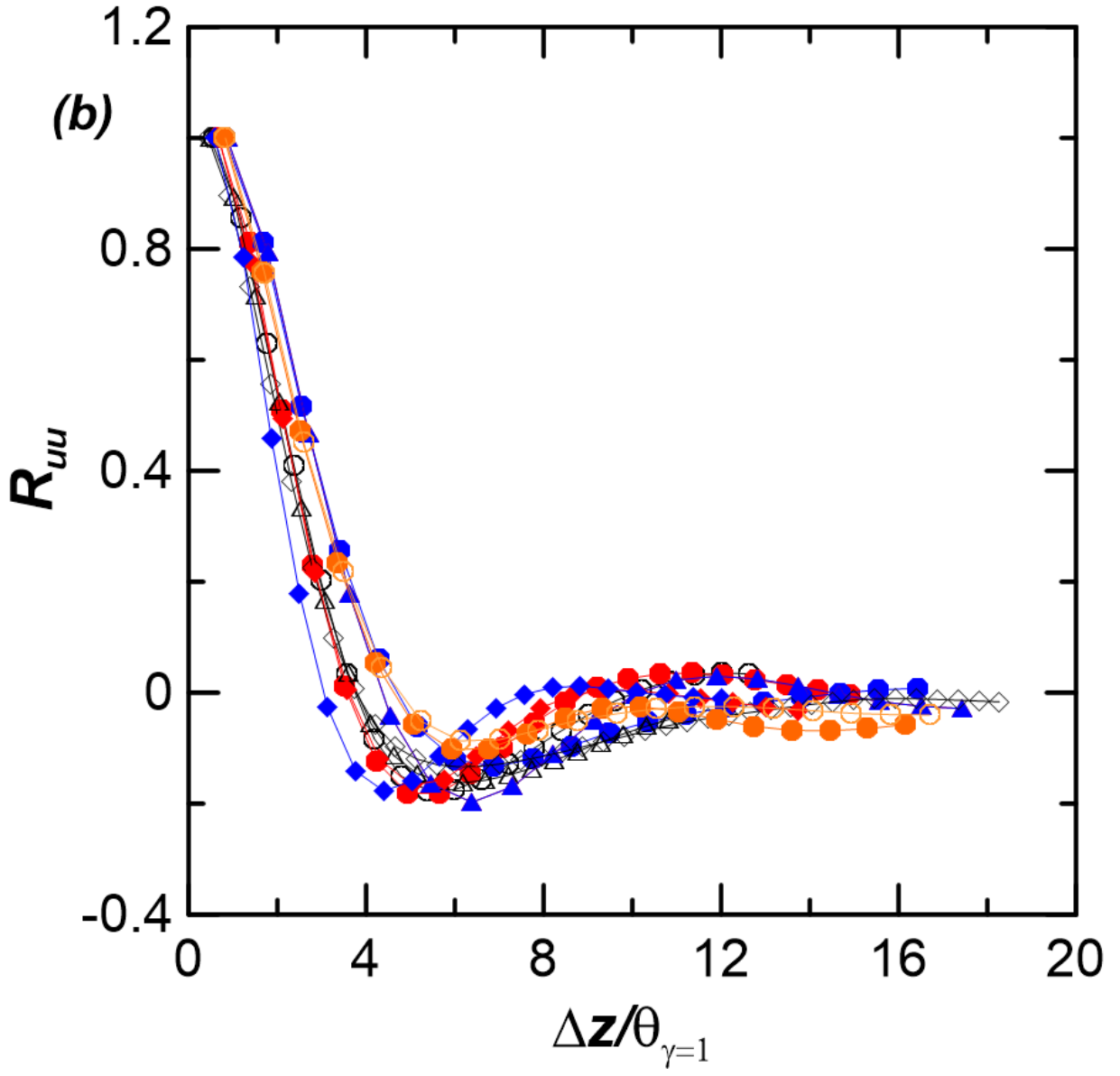
This is the author's peer reviewed, accepted manuscript. However, the online version of record will be different from this version once it has been copyedited and typeset.

PLEASE CITE THIS ARTICLE AS DOI: 10.1063/1.50063948



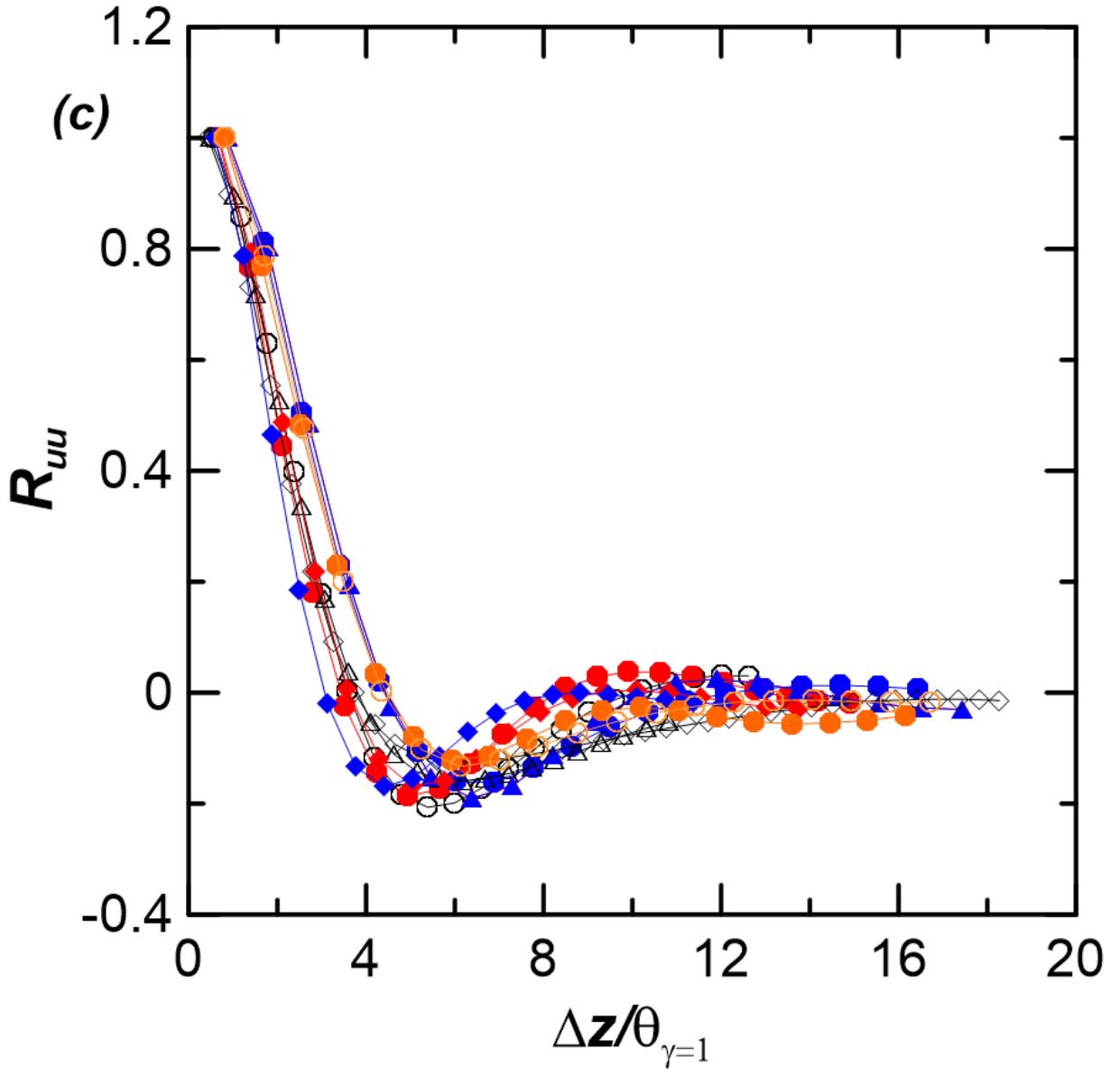
This is the author's peer reviewed, accepted manuscript. However, the online version of record will be different from this version once it has been copyedited and typeset.

PLEASE CITE THIS ARTICLE AS DOI: 10.1063/1.50063948



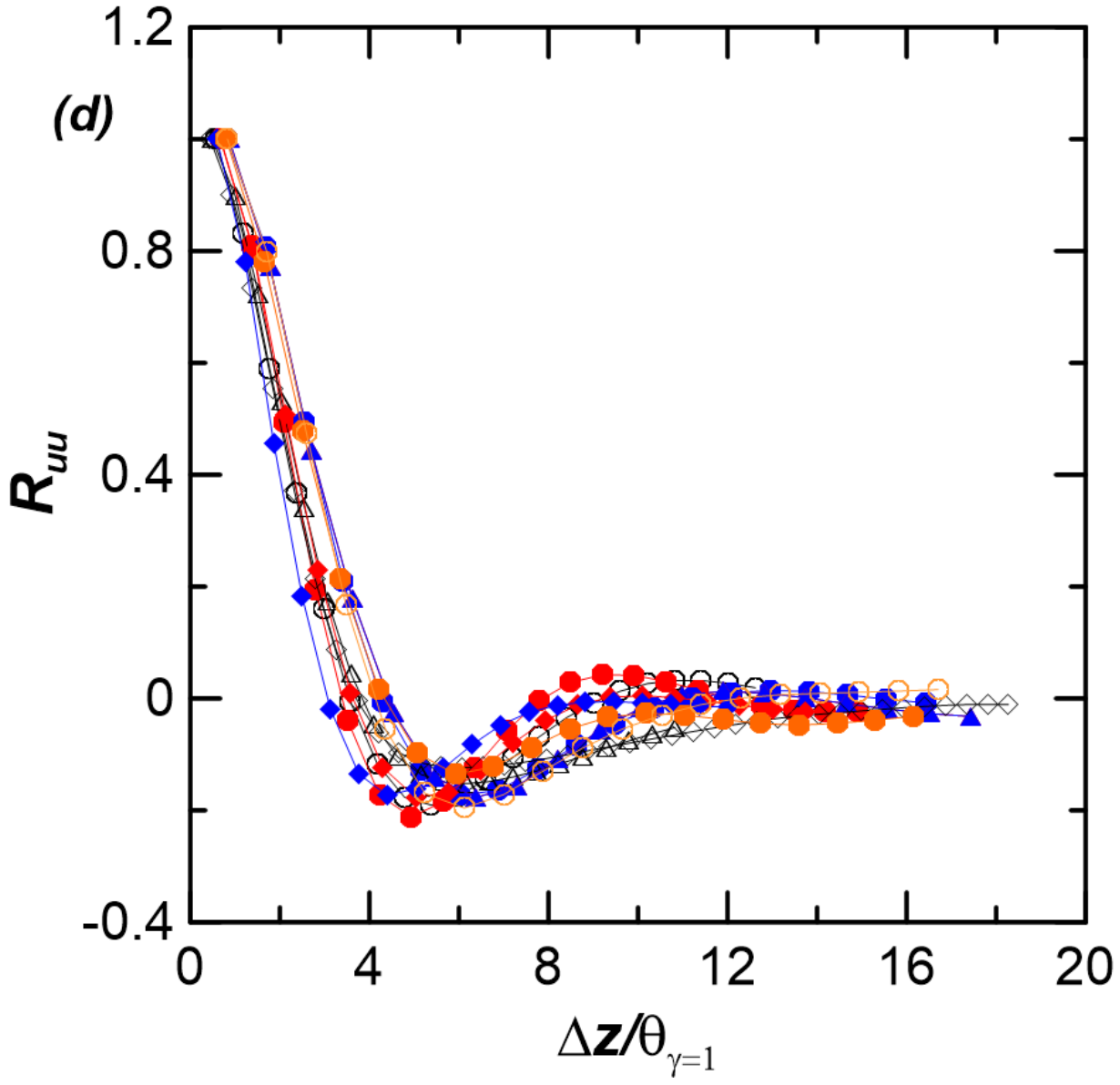
This is the author's peer reviewed, accepted manuscript. However, the online version of record will be different from this version once it has been copyedited and typeset.

PLEASE CITE THIS ARTICLE AS DOI: 10.1063/1.50063948



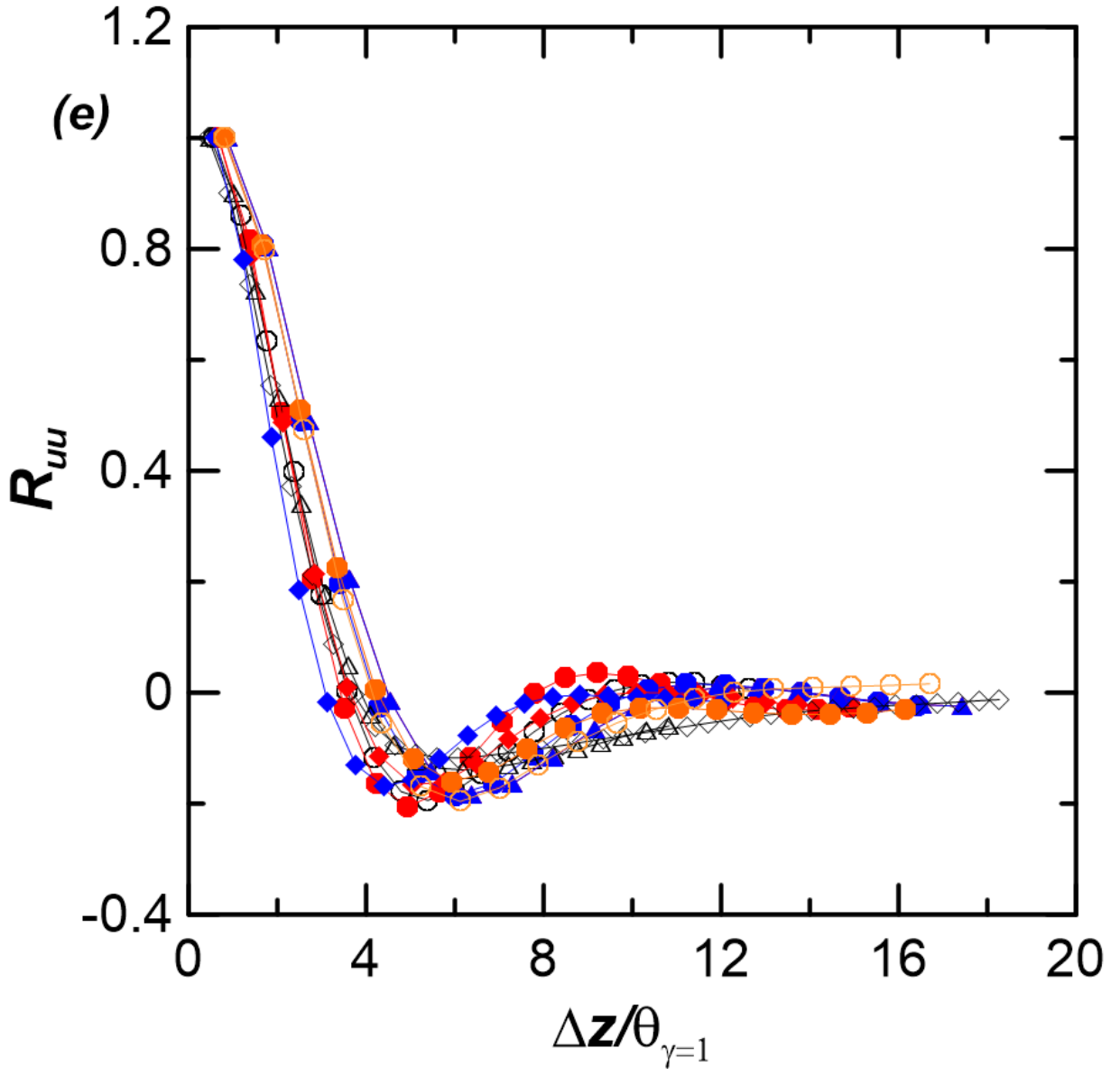
This is the author's peer reviewed, accepted manuscript. However, the online version of record will be different from this version once it has been copyedited and typeset.

PLEASE CITE THIS ARTICLE AS DOI: 10.1063/1.50063948



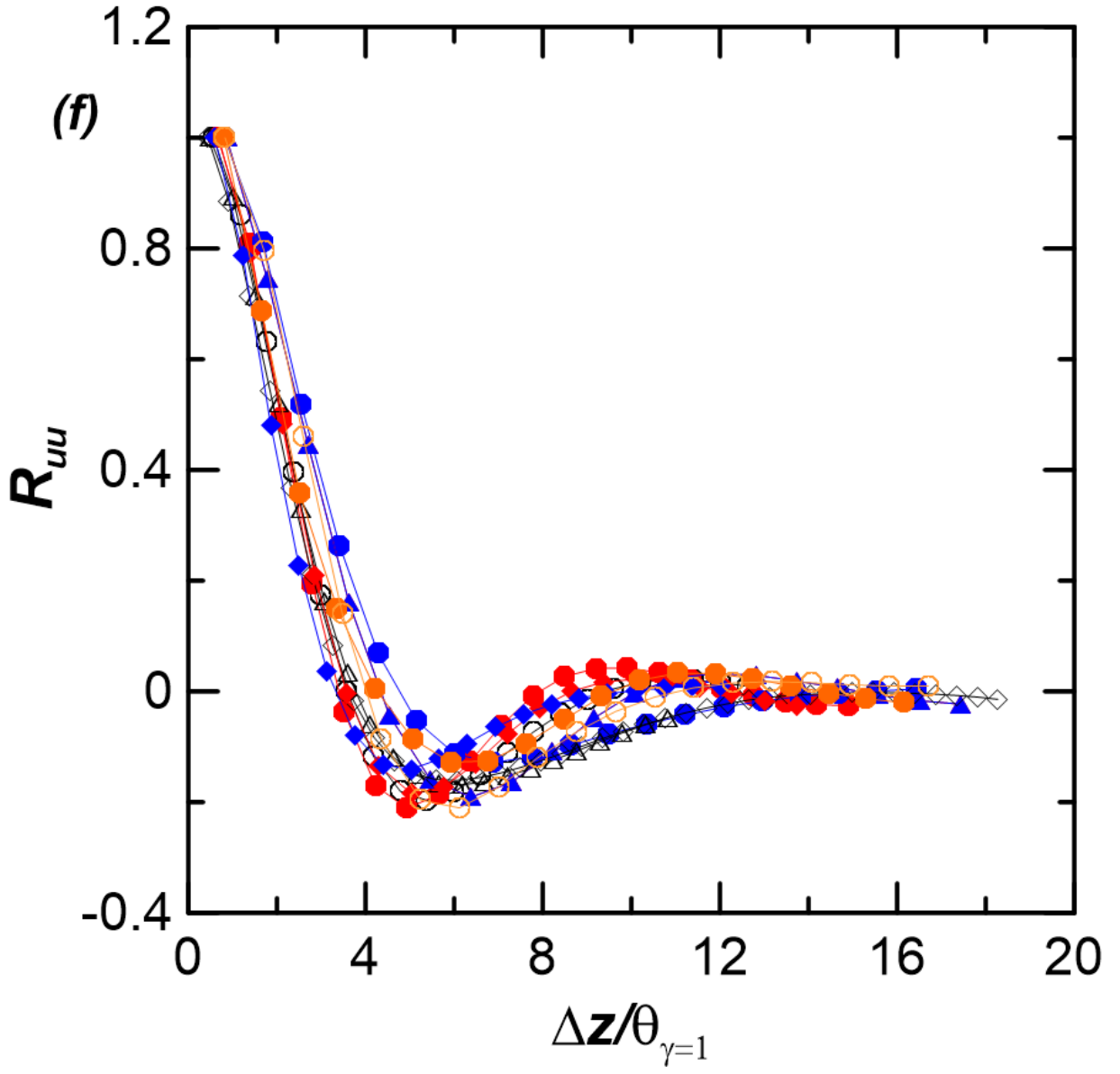
This is the author's peer reviewed, accepted manuscript. However, the online version of record will be different from this version once it has been copyedited and typeset.

PLEASE CITE THIS ARTICLE AS DOI: 10.1063/1.50063948

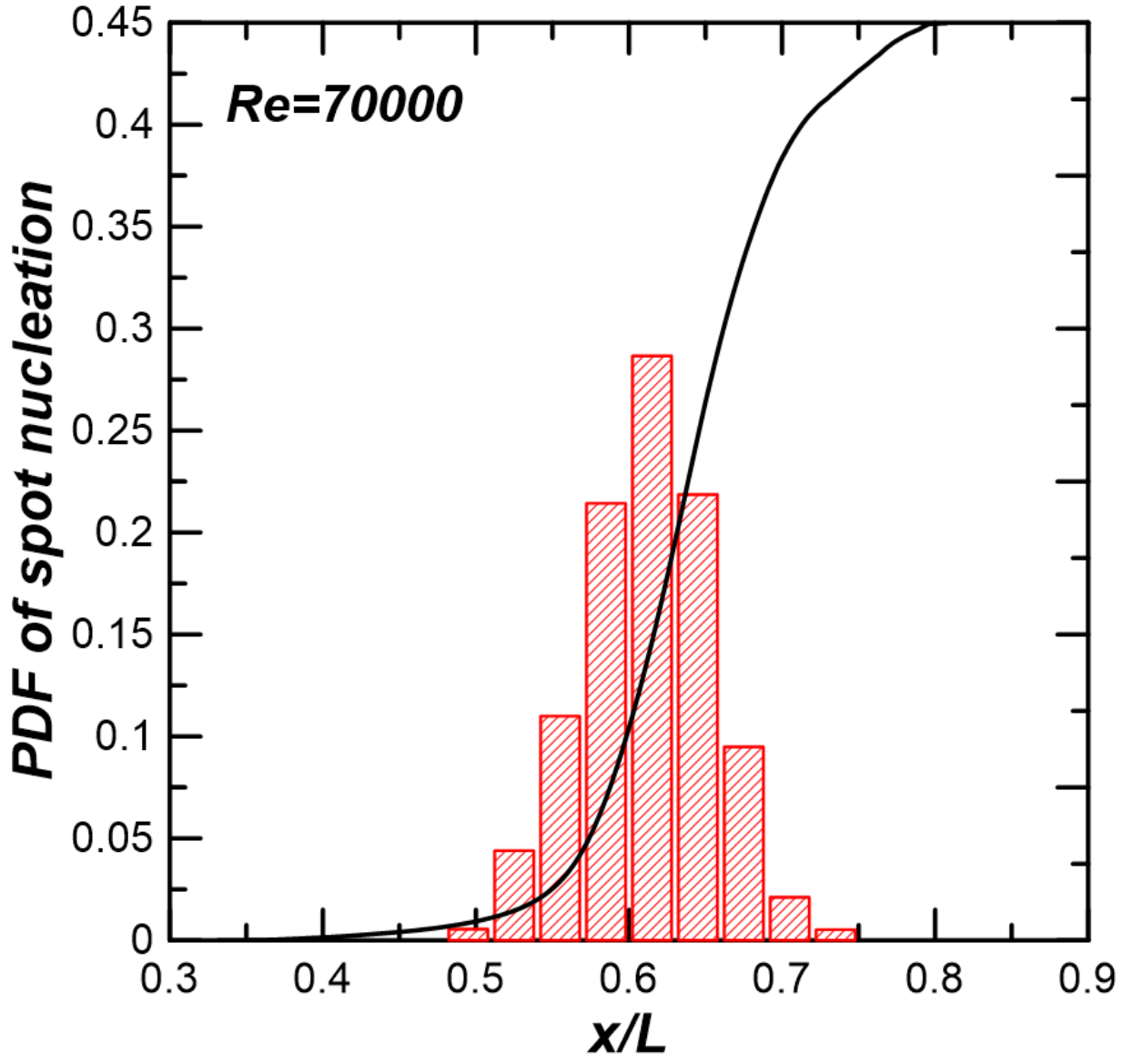


This is the author's peer reviewed, accepted manuscript. However, the online version of record will be different from this version once it has been copyedited and typeset.

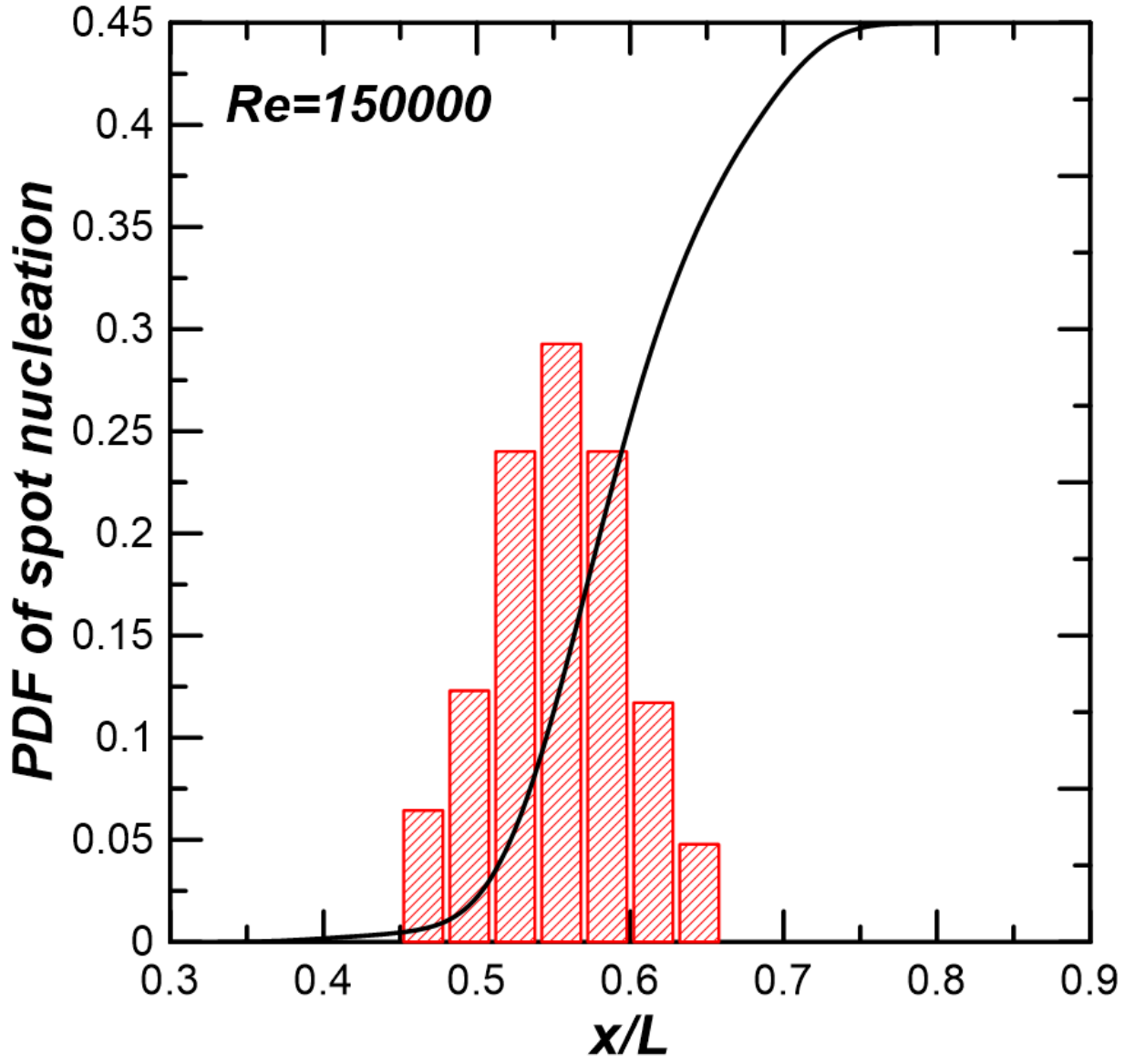
PLEASE CITE THIS ARTICLE AS DOI: 10.1063/1.50063948



This is the author's peer reviewed, accepted manuscript. However, the online version of record will be different from this version once it has been copyedited and typeset.
PLEASE CITE THIS ARTICLE AS DOI: 10.1063/5.0063948

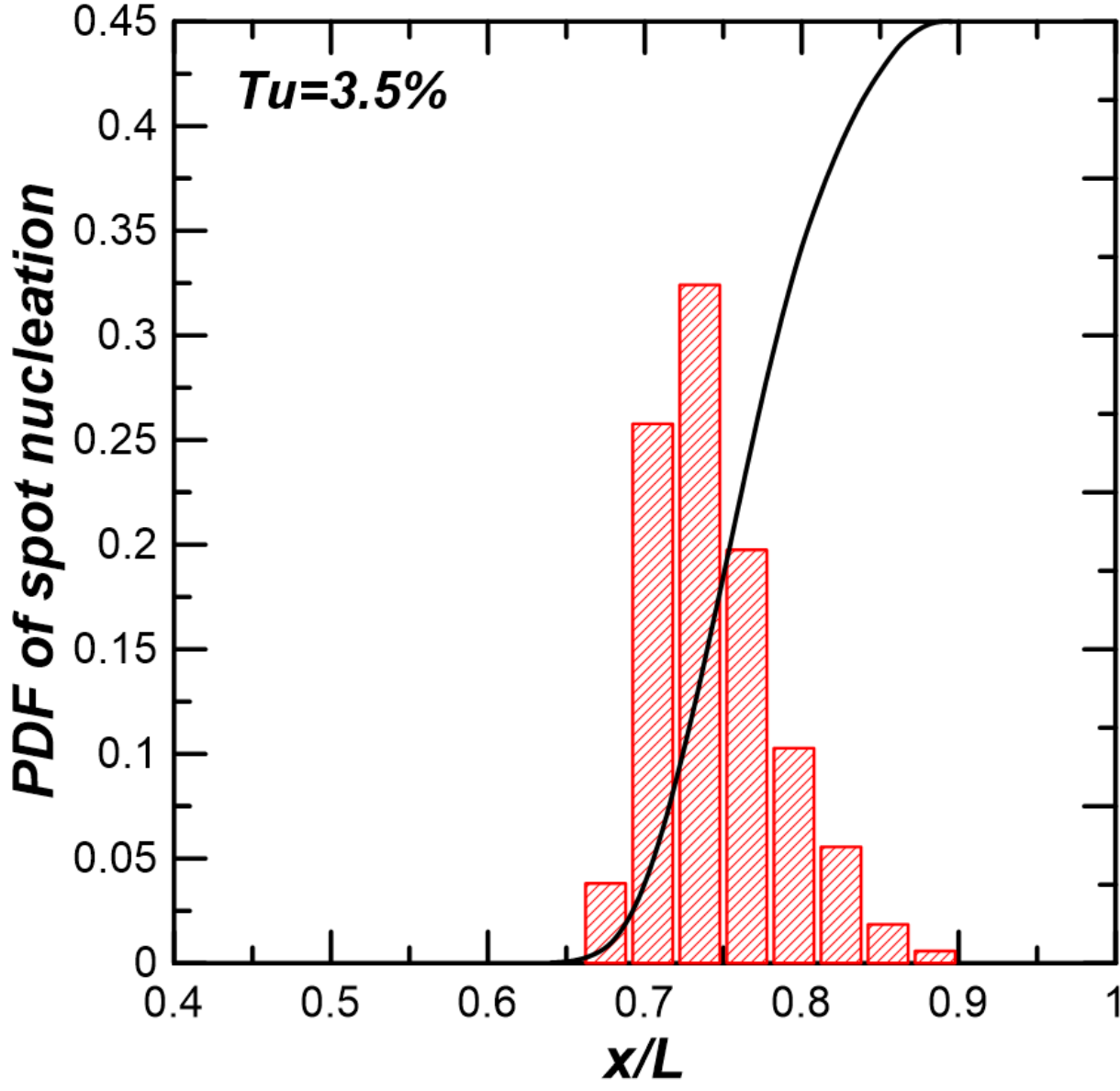


This is the author's peer reviewed, accepted manuscript. However, the online version of record will be different from this version once it has been copyedited and typeset.
PLEASE CITE THIS ARTICLE AS DOI: 10.1063/5.0063948



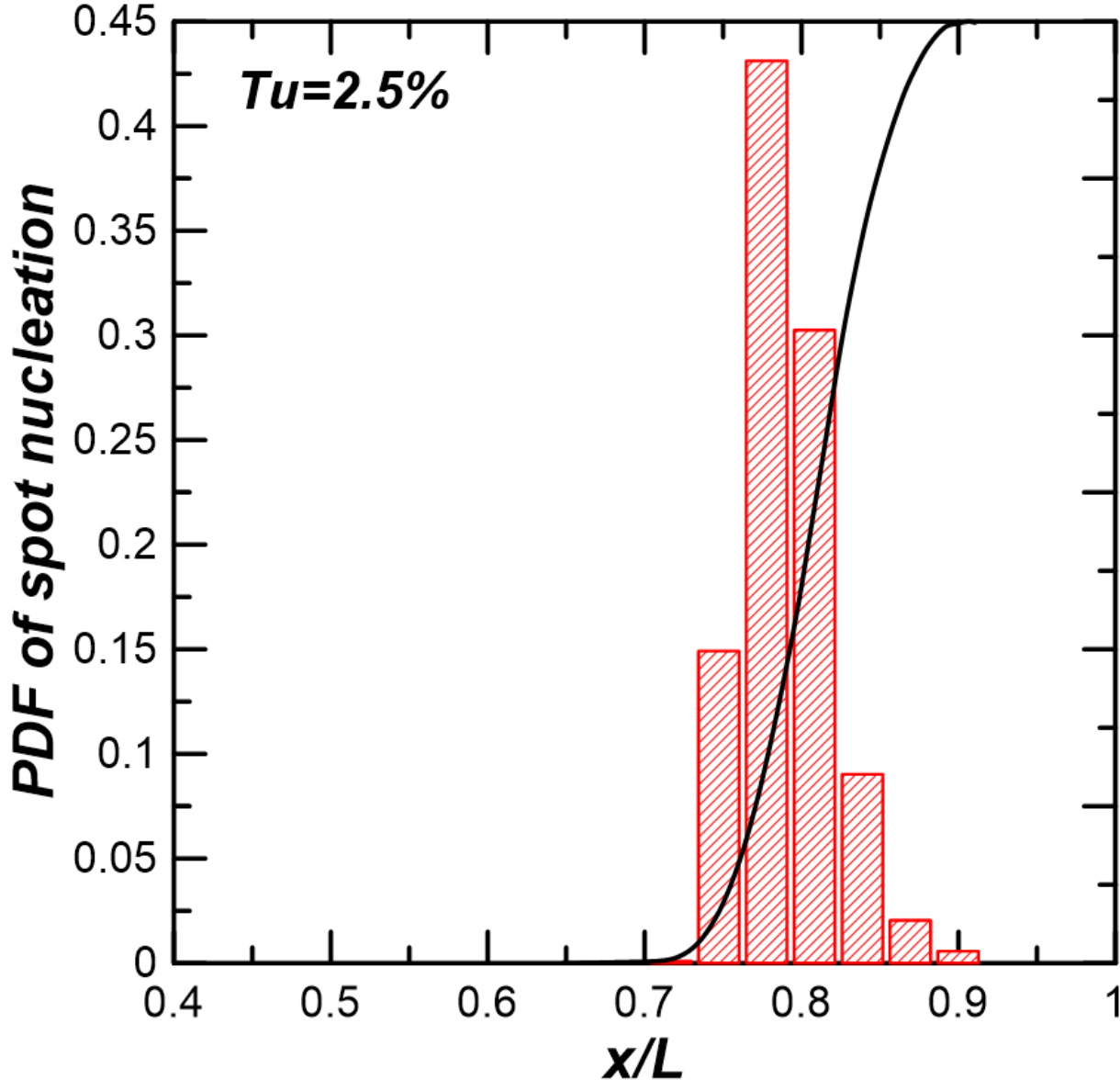
This is the author's peer reviewed, accepted manuscript. However, the online version of record will be different from this version once it has been copyedited and typeset.

PLEASE CITE THIS ARTICLE AS DOI: 10.1063/5.0063948



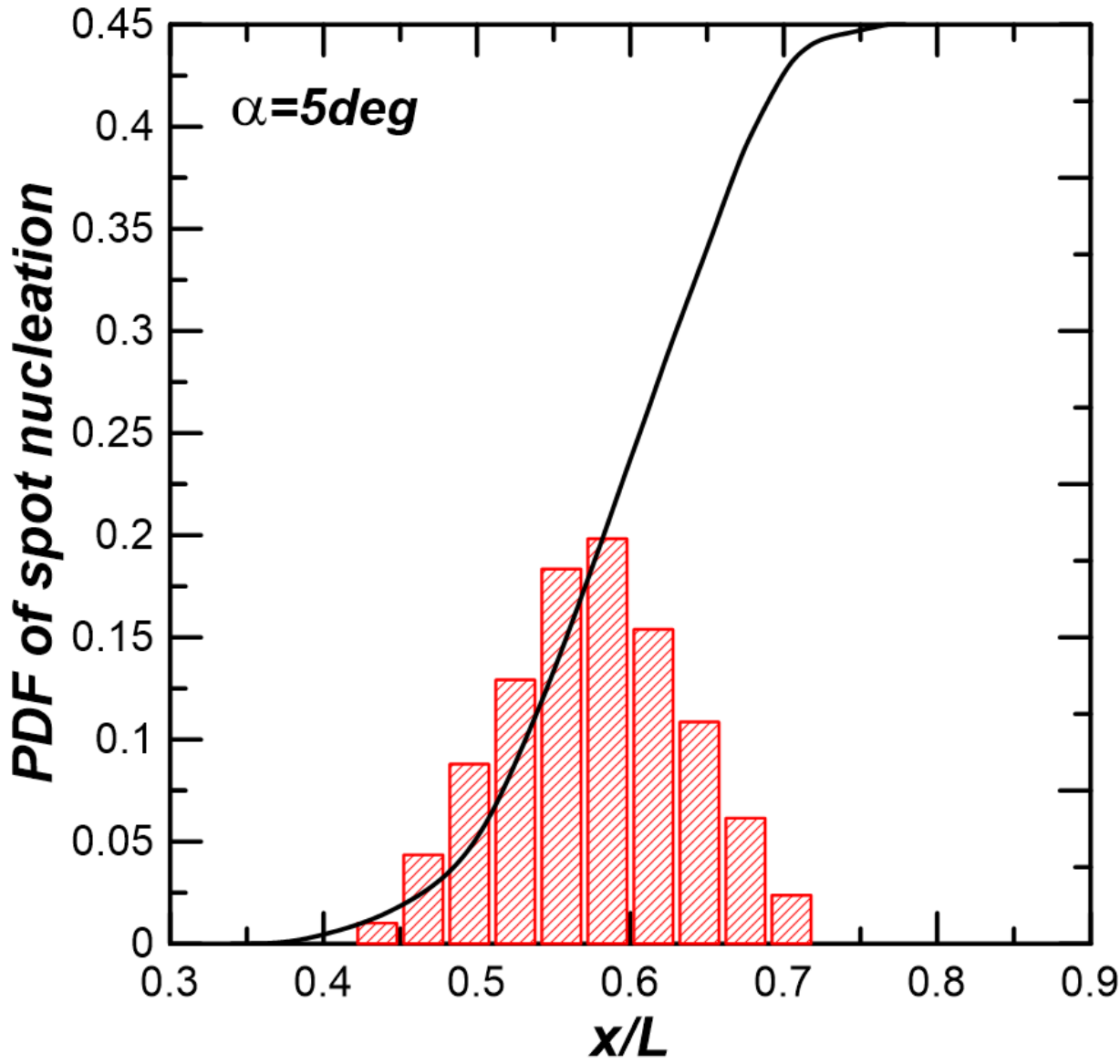
This is the author's peer reviewed, accepted manuscript. However, the online version of record will be different from this version once it has been copyedited and typeset.

PLEASE CITE THIS ARTICLE AS DOI: 10.1063/5.0063948



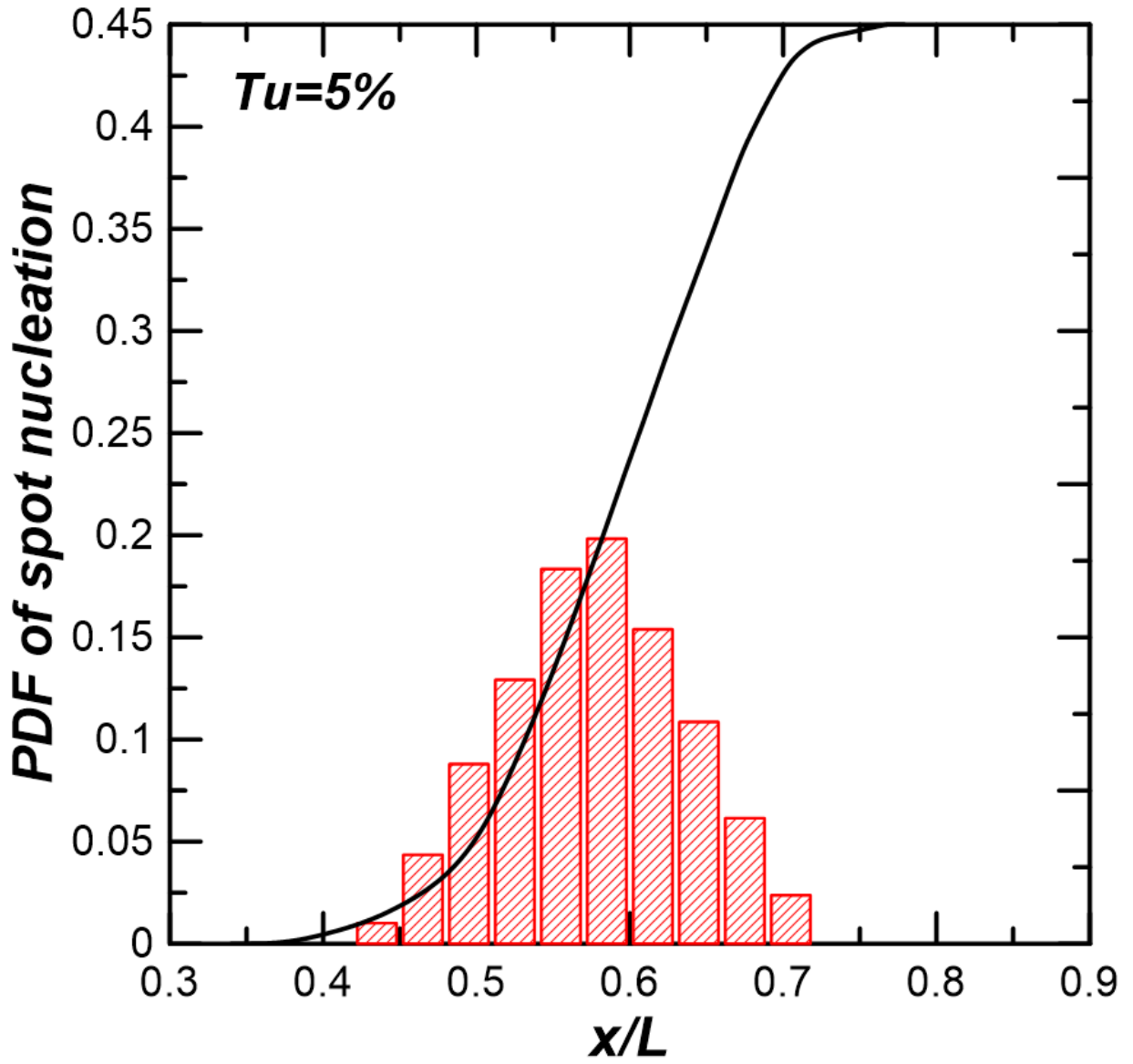
This is the author's peer reviewed, accepted manuscript. However, the online version of record will be different from this version once it has been copyedited and typeset.

PLEASE CITE THIS ARTICLE AS DOI: 10.1063/5.0063948



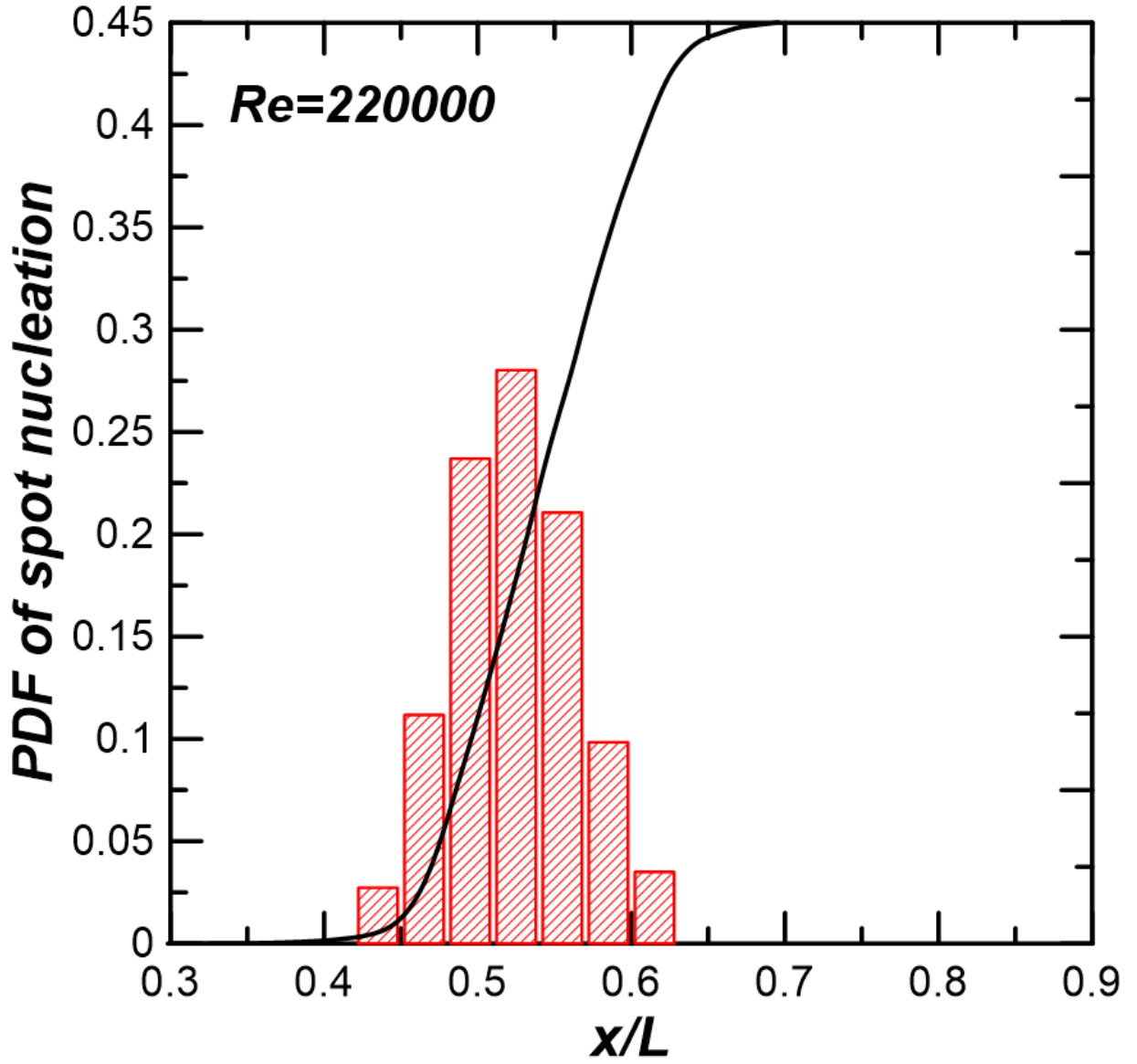
This is the author's peer reviewed, accepted manuscript. However, the online version of record will be different from this version once it has been copyedited and typeset.

PLEASE CITE THIS ARTICLE AS DOI: 10.1063/1.50063948



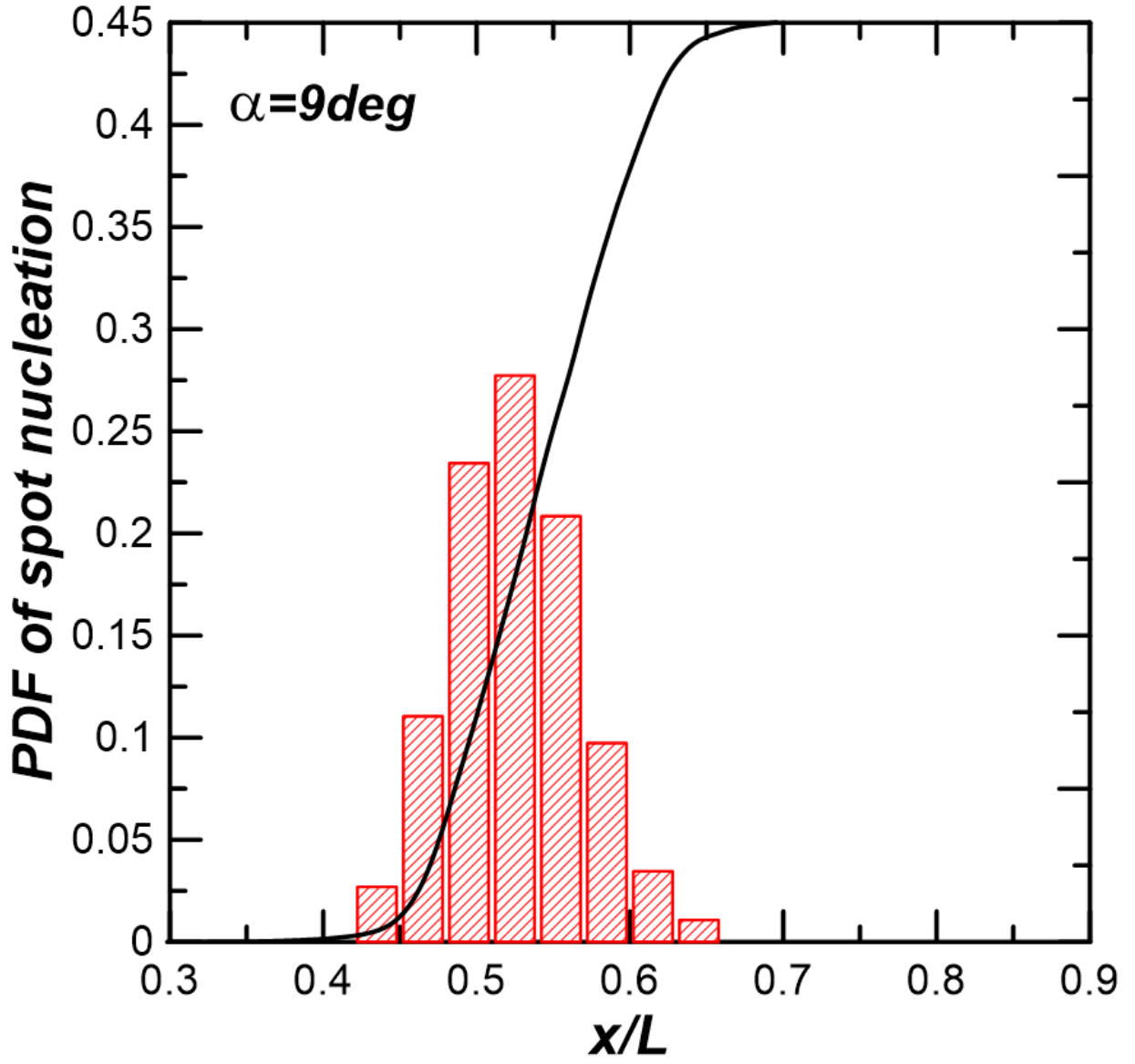
This is the author's peer reviewed, accepted manuscript. However, the online version of record will be different from this version once it has been copyedited and typeset.

PLEASE CITE THIS ARTICLE AS DOI: 10.1063/1.50063948

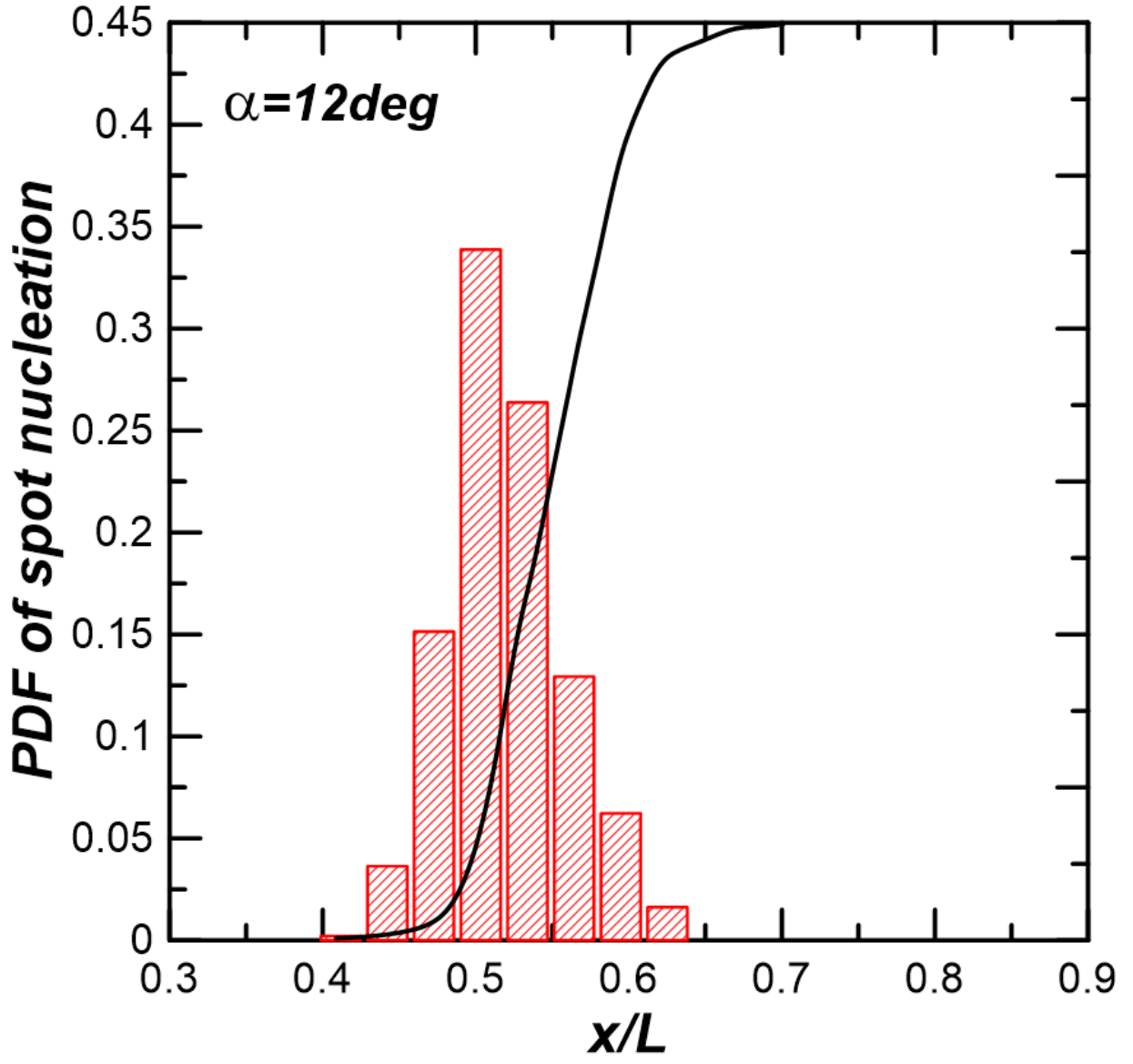


This is the author's peer reviewed, accepted manuscript. However, the online version of record will be different from this version once it has been copyedited and typeset.

PLEASE CITE THIS ARTICLE AS DOI: 10.1063/1.50063948



This is the author's peer reviewed, accepted manuscript. However, the online version of record will be different from this version once it has been copyedited and typeset.
PLEASE CITE THIS ARTICLE AS DOI: 10.1063/5.0063948



This is the author's peer reviewed, accepted manuscript. However, the online version of record will be different from this version once it has been copyedited and typeset.

PLEASE CITE THIS ARTICLE AS DOI: 10.1063/1.50063948

